Journal of Marine Science and Engineering

MDPI

Article

Scour near Offshore Monopiles, Jacket-Type and Caisson-Type Structures

L. C. van Rijn [1,*], N. Geleynse [2], L. Perk [2] and D. Schoonhoven [2]

[1] LVRS-Consultancy, Domineeswal 6, 8356DS Blokzijl, The Netherlands
[2] WaterProof-Consultancy, IJsselmeerdijk 2, 8221RC Lelystad, The Netherlands; nathanael.gelynse@waterproofbv.nl (N.G.); luitze.perk@waterproofbv.nl (L.P.)
* Correspondence: info@leovanrijn-sediment.com

Abstract: Scour near various offshore structures (monopile, caisson foundation and jacket structure) was studied by performing laboratory flume tests and numerical solutions with a semi-empirical model (SEDSCOUR) and a sophisticated 2DV model (SUSTIM2DV). The laboratory test results show that the maximum free scour depth around a monopile without bed protection is slightly higher than the pile diameter. The maximum scour consisting of pile scour and global scour around an open jacket structure standing on four piles is much lower than the scour near the other structures (monopile and caisson). The maximum scour depth along a circular caisson foundation is found to be related to the base diameter of the structure. The main cause of the scour near these types of structures is the increase in the velocity along the flanks of the structure. Six cases have been used for validation: two laboratory cases (A and B) and four field cases (C, D, E and F). The measured scour values of the new physical model tests with the monopile and the open jacket structure presented in this paper are in reasonably good agreement with other laboratory and field scour data from the literature. The semi-empirical SEDSCOUR model proposed in this paper can be used for the reliable prediction of free scour and global scour near monopiles and jacket structures in a sandy bed (even with a small percentage of mud, up to 30%). The maximum scour depth along a large-scale caisson structure is more difficult to predict because the scour depth depends on the precise geometry and dimensions of the structure and the prevailing flow and sediment conditions. A detailed 2DV model with a fine horizontal grid (2 m) along a stream tube following the contour of the caisson is explored for scour predictions. The 2DV model simulates the flow and sediment transport at 50 to 100 points over the depth along the stream tube and can be run on a time-scale of 1 year.

Keywords: scour near offshore structures; prediction models for scour

Academic Editor: Fuping Gao

Received: 15 December 2024
Revised: 27 January 2025
Accepted: 27 January 2025
Published: 30 January 2025

Citation: van Rijn, L.C.; Geleynse, N.; Perk, L.; Schoonhoven, D. Scour near Offshore Monopiles, Jacket-Type and Caisson-Type Structures. *J. Mar. Sci. Eng.* **2025**, *13*, 266. https://doi.org/10.3390/jmse13020266

1. Introduction

1.1. General

Many countries in coastal regions plan to utilize their offshore wind potential by developing offshore wind farms in water depths of 20 to 50 m. On a global level, Europe is still a market leader in offshore wind project construction (about 50%), followed by Asia (about 45%) and the US (5%). Various types of foundation structures of offshore wind turbines are used: monopiles, gravity-based structures and jacket/tripod structures.

The monopile is the most applied foundation type in shallow waters with a sandy soil covered with migrating sand waves. Gravity-based structures (GBSs; caisson-type foundation structures) are suitable for wind turbines in shallow waters (up to 30 m) with sandy and rocky type soils. These types of structures generally have skirts with lengths of 2 to 3 m under the foundation structure to prevent undermining. Jacket-type structures can be used in deeper waters with depths up to 50 m. The scour near various types of structures is discussed in Sections 1.2–1.4. Experimental and numerical methods are presented in Section 2. The new experimental results are analyzed in Sections 3 and 4. Scour models and prediction results are given in Section 5. Summary and conclusions are given in Section 6.

1.2. Scour Around Monopiles

Many data sets of free scour around monopiles in laboratory and field conditions are available. Early work on this by Breusers et al. [1], Melville [2], Melville-Sutherland [3], Kothyari et al. [4], Melville [5], Lim [6], Melville and Coleman [7] goes back to current-related scour near circular bridge piers. They and others have found maximum scour depth values ($d_{s,max}$) in the range of 0.5 to 2 of the pile's diameter (D_{pile}), expressed as $d_{s,max} = 0.5$ to 2 D_{pile}, depending on water depth, flow conditions, sediment size and other factors. Cefas [8] measured a maximum scour depth of up to 5 m around the monopiles ($D_{pile} = 4.2$ m; $d_{s,max} = 1.1\ D_{pile}$) of an offshore wind farm within coastal waters, in Scroby Sands, off Great Yarmouth (east coast of England). Similar values are reported by Rudolph et al. [9] for the Q7 wind farm at 20 km offshore of Holland's coast and Raaijmakers et al. [10] for the wind farm Luchterduinen, offshore near Holland's coast.

1.3. Scour Around Gravity-Based Structures

Assessments on scour depth around circular gravity-based structures in laboratory conditions were performed by [11–16]. Whitehouse [11] measured maximum scour depth values of 0.2 to 0.5 times the base foundation diameter ($d_{s,max}/D_{base} = 0.2$–0.5) along circular caisson structures with long skirts (9.5 m) for high-current velocities ($u_o/u_{cr} = 4$ to 6), where u_o = the free-stream velocity upstream of the structure and u_{cr} = the critical current velocity of motion of the sand seabed. Tavouktsoglu [15] measured values of $d_{s,max}/D_{base} = 0.3$–0.65 for low-current velocities ($u_o/u_{cr} \cong 1.2$). Sarmiento et al. [16] measured a maximum scour depth along a caisson structure of about $d_{s,max} = 0.125\ D_{base}$ after 5 h in a movable bed scale model ($d_{50} = 0.15$ mm), with a water depth of 1 m and a current velocity of 0.42 m/s ($u_o/u_{cr} \cong 2$). Whitehouse et al. [12] have summarized scour data for two field cases with gravity-based structures (GBSs). The values of $d_{s,max}/D_{base}$ are in the range of 0.05 to 0.12 for $u_{o,max}/u_{cr} = 4$ to 5. Overall, the measured range is $d_{s,max}/D_{base} = 0.05$ to 0.65, which is a rather large range, indicating that the scour near GBS is sensitive to the structure's precise dimensions, flow and sediment conditions.

1.4. Scour Around Jacket-Type Structures

Scour data near jacket-type structures are relatively scarce. Rudolph et al. [17] studied the scour near a jacket structure (open structure of multiple piles/legs) at block L9 of the Dutch North Sea sector, which was installed in the summer of 1997. The piles resting in the seabed ($d_{50} = 0.2$ mm) have a diameter of D_{pile} in the range of 1.2 to 1.5 m. Typical depth-averaged peak flow velocities are 0.5 m/s during spring tide. Maximum far-field scour depths were measured in the range of 1.5 to 5.0 m, and the near-field scour near the legs/piles (D_{pile}) was in the range of 2.0 to 3.5 m (about 1.5 to 2.5 D_{pile}). The far-field scour hole (extent of bathymetrical changes relative to the undisturbed situation) had a radius of roughly 2.5 to 3 times the pile spacing. Bolle et al. [18] and Baelus et al. [19] analyzed scour depth around the jacket structure at Thorton Bank offshore wind park in the

southern North Sea. The maximum scour depth was in the range of $d_{s,max} = 0.3$ to $0.9\ D_{pile}$. Welzel et al. [20,21] studied near-field and far-field scour around a jacket structure in a wave-current basin with a water depth of 0.67 m (scale 1 to 30) and a sand d_{50} of 0.19 mm. The structure has four legs with pile diameter of 1.2 m. Current velocities varied between 0.1 and 0.4 m/s. The maximum far-field scour depth around the structure was about 1 m or $d_{s,max} = 0.8\ D_{pile}$ for current-only conditions. The maximum near-field scour depths around the least- and the most-exposed piles was $d_{s,max} = 1.3$ to $1.75\ D_{pile}$ for current-only conditions. Other types of jacket structures were also studied by Welzel et al. 2020, 2024 [22,23]. Zhang et al., 2025 [24] used a 3D flow model to compute the near-bed flow and turbulence characteristics around a jacket structure. An overview of the most relevant and recent scour-related research of various types regarding offshore structures are given by Chambel et al. [25] and Sarmiento et al. [16].

2. Experimental and Numerical Methods

The prediction of the scour depth around these types of foundation structures in offshore conditions requires the application of numerical simulation models in combination with experiments in physical scale models. Both types of modelling tools are discussed in this paper.

New exploring experiments in a wide recirculating flume with steady flow conditions were performed to determine the scour hole dimensions around a monopile, a jacket structure with 4 legs and a gravity structure (caisson-type structure with a monopile on top). The experiments were performed in a small basin (length = 10 m; width = 1.3 m) at the WaterProof laboratory. The hydrodynamic data (flow field) were measured above a fixed model bottom (non-mobile) to acquire steady initial conditions during all velocity measurements (detailed mapping of the initial flow field). The bed roughness of the non-mobile bed is about 0.5 mm (cemented sand bed; $k_s \cong 3\ d_{90}$; $d_{90} = 0.18$ mm, see below). The water depth was about 0.35 m. The depth-averaged approach current velocity was about 0.26 m/s. The velocity profile at various locations around each structure was measured using a 3D NORTEK Vectrino instrument (Nortek, Hoofddorp, The Netherlands). Measured velocity profiles above the non-mobile bed upstream of the structures are very similar to the measured velocity profiles above the mobile sand bed upstream of the structures (measured during scour tests). In addition, streamlines were visualized using surface floats consisting of a small piece of wood with an aluminum body (cross) attached to a short vertical line of 5 cm so that the float represents the velocity at 5 cm under the watersurface. All dimensions and conditions are given in Table 1 (see also the photographs in Section 4).

After the flow experiments with a fixed bed, scour experiments were performed in the basin with a mobile sediment bed consisting of medium-fine sand ($d_{50} = 0.1$ mm; $d_{90} = 0.18$ mm; critical depth-averaged velocity for initiation of motion; $u_{cr} = 0.2$ m/s). The depth-averaged approach velocity was slightly above the critical velocity ($u_o/u_{cr} = 1.3$). This represents live-bed scour, although the sand transport and scour upstream of the structure was minimum. Each test was run until the maximum scour depth remained approximately stable and reached equilibrium. The test duration was 6.5 h for the test with a monopile; it was 6.5 h for the test with a caisson structure (test was stopped after the tipping over of the caisson structure after 6.5 h) and 20 h for the test with a jacket structure. The scour depth data were derived from 3D photographs after drying the model and from mechanical pointer gages.

Table 1. Basic data of scour experiments; d_{50} = 0.1 mm.

Parameter	Monopile	Caisson with Monopile (GBS)	Jacket Structure
Structure dimensions	D_{pile} = 0.11 m (pile diameter)	$D_{caisson}$ = 0.32 m; D_{pile} = 0.11 m $h_{caisson}$ = 0.1 m; h_{skirt} = 0.035 m (caisson was placed on top of bed; skirt was in the bed)	D_{leg} = 0.02 m $D_{crossmember}$ = 0.01 m L_{base} = 0.365 m (distance legs)
Water depth	0.35 m	0.35 m	0.35 m
Upstream current	0.26 m/s	0.27 m/s	0.26 m/s

The flow field and the scour details of these experiments are presented and used for the validation of the scour models. Two types of scour prediction models were used: (1) the semi-empirical scour model SEDSCOUR and (2) the sophisticated SUSTIM2DV-model. Both models were developed by LVRS-Consultancy and are explained in Section 5.

3. Experimental Results of Flow Around a Monopile, Jacket Structure and Gravity-Based Structure

Figures 1–3 show the measured velocity profiles at various locations for the monopile, GBS and jacket-type structure, respectively. The most characteristic features include the following:

- *monopile*: a significant increase in the approach depth-averaged flow velocity from 0.26 m/s at P1 to about 0.35 m/s at the flanks of the pile at P2 and P3; the velocity profile is quite uniform over depth (accelerated flow);
- *caisson with monopile on top*: a significant increase in the approach depth-averaged flow velocity from 0.26 m/s at P1 to about 0.35 m/s on the flank of the caisson at P2, decreasing for larger lateral distances (0.32 m/s at P5); the velocity profile is rather uniform at P2, and the velocity profile at P1 is slightly distorted, most likely due to the effect of the downward-directed flow at the base of the structure;
- *jacket structure*: an increase in the approach depth-averaged flow velocity from 0.26 m/s at P1 to about 0.30–0.33 m/s at P7 and P8, lateral of the structure; the vertical distribution of the flow velocities is rather similar.

It is noted that the increase in the velocities measured on the side of the structures is somewhat too high (about 10%) due to the blocking effect (limited width of the flume).

Figure 4 shows flow lines based on near-surface floats. The flow lines are fairly straight for the open jacket structure and curvier for the monopile and the caisson with a pile on top.

Figure 5 shows the dimensionless depth-averaged velocity along the structure (monopile and caisson) and in the axis downstream of the jacket structure. L is the structure's length being L = 0.11 m for the monopile, L = 0.32 m (base diameter) for the caisson structure and L = 0.38 m (base length) for the jacket structure. The x-coordinate is the distance along a line from the upstream structure face in the centreline around the perimeter of the structure that ends in the downstream structure face in the centreline and then following the centreline. The first point is at 0.055 m from the upstream structure face for the monopile, 0.16 m for the caisson and 0.19 m for the jacket structure. The measured values along the centreline behind the structures are the depth-averaged velocities derived from the measurements in the centreline (no averaging over the width). The upstream depth-averaged current velocity is 0.26–0.27 m/s for all structures. The current velocity strongly increases in the acceleration zone ($0 < x/L < 0.5$) with a maximum value of about $u/u_o \cong 1.4$ for the monopile and decreases (maximum 40%) in the lee zone of the monopile. Miles et al. 2017 [26] report a reduction of about 50%. They also report that the flow velocity

returned to within 5% of the free-stream velocity at about 8 to 9 D_{pile} of the pile centre. The re-adjustment distance to free-stream velocities downstream of the monopile is about x/L ≅ 15–20 for the monopile of this study. A similar re-adjustment distance of x/L ≅ 15–20 seems present for the caisson-type structure. For the jacket-type structure, this re-adjustment seems much shorter because the flow interference is much less.

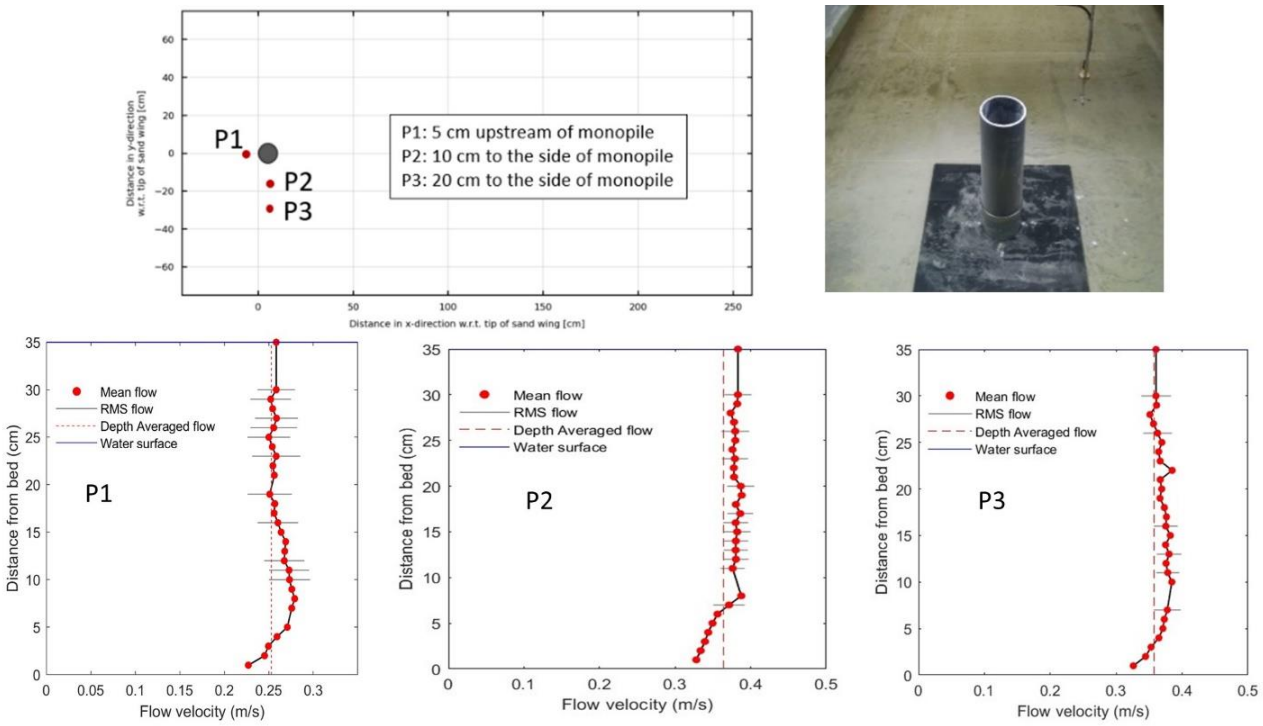

Figure 1. Flow velocity field around the monopile (D_{pile} = 0.11 m).

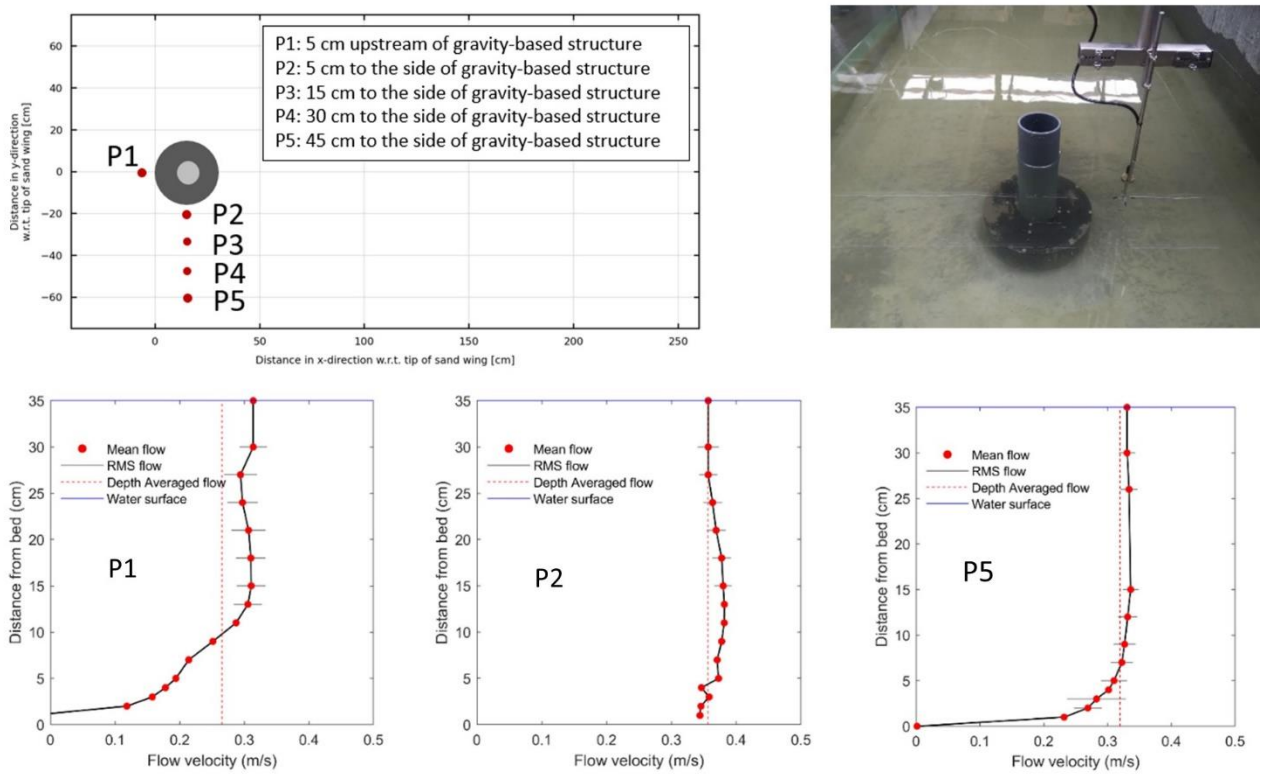

Figure 2. Flow velocity field around the caisson structure ($D_{caisson}$ = 0.32 m) with a monopile on top (D_{pile} = 0.11 m).

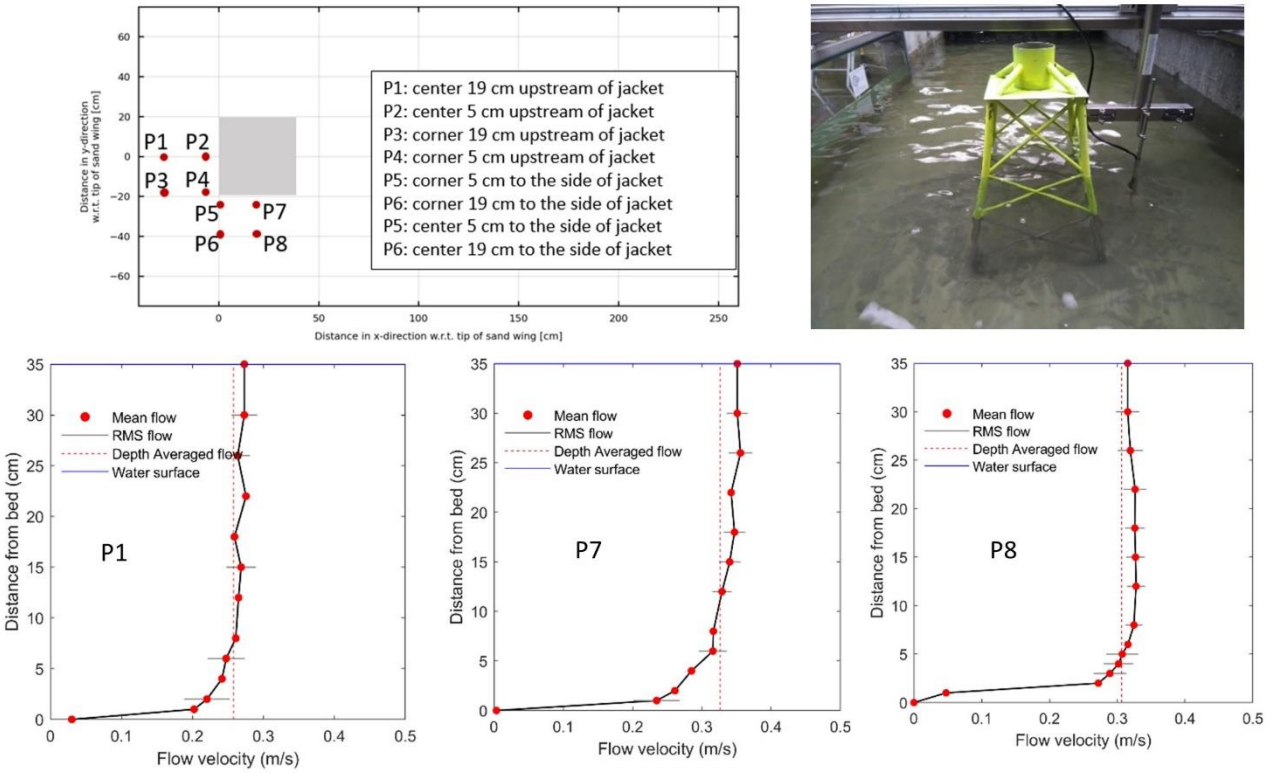

Figure 3. Flow velocity field around the jacket structure (D_{leg} = 0.02 m; distance between legs = 0.365 m).

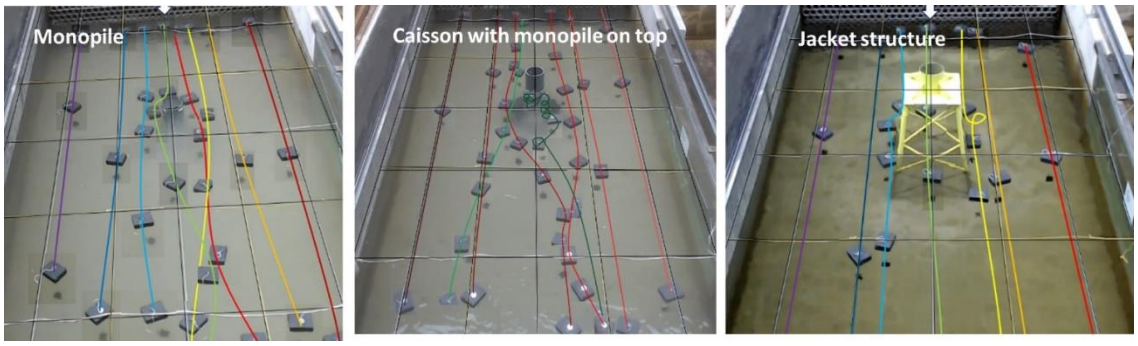

Figure 4. Flow lines for the 3 main experiments, obtained from tracking the position of near-surface floats (flow from top to bottom).

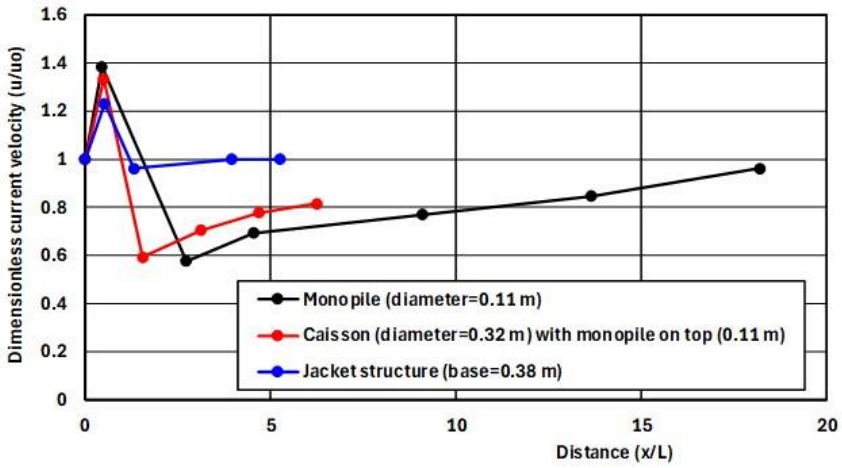

Figure 5. Dimensionless depth-averaged velocity as a function of dimensionless distance along the structure.

4. Experimental Results of Scour near the Monopile, Jacket Structure and Gravity-Based Structure

4.1. Experimental Scour Results

The scour results for the three structures are presented in Table 2 and in Figures 6–9. The most important scour characteristics are as follows:

- *monopile*: the maximum scour depth is $d_{s,max} \cong 1.1\ D_{pile}$ after 5 h with a maximum scour length of $L_{s,max} \cong 3\ D_{pile}$ at both sides; the maximum scour depth after 6.5 h is almost the same;
- *caisson with monopile on top*: the maximum scour depth is $d_{s,max} \cong 1\ h_{caisson}$ (height of the caisson) after 6.5 h (just before the tipping over of the structure due to scour undermining, see Figure 6); the maximum scour length is $L_{s,max} \cong 1\ D_{caisson}$ at both sides;
- *jacket structure*: the maximum scour depth near the legs is $d_{s,max} \cong 2.5\ D_{leg}$ after 10 h; the maximum scour depth after 20 h is almost the same; the maximum scour length is $L_{s,max} \cong 10\ D_{leg}$ at both sides; scour in the centre part under the structure is lower (≅50% of scour depth near legs).

Table 2. Measured data from scour experiments; $d_{50} = 0.1$ mm.

Parameter	Monopile	Caisson with Monopile (GBS)	Jacket Structure
Maximum scour depth	0.12 m (≅1.1 D_{pile})	0.10 m (≅1.0 $h_{caisson}$) (0.3 $D_{caisson}$)	0.05 m near legs (≅ 2.5 D_{leg}) 0.03 m (≅ 1.5 D_{leg}) in middle structure
Maximum scour length	0.35 m (≅3 D_{pile}) on both sides of pile	0.3 m (1 $D_{caisson}$) on both sides	0.20 m (≅10 D_{leg}) on both sides of leg

4.2. Discussion

Monopile structure: **T**he maximum scour depth of the present tests with a monopile ($d_{s,max} = 1.1\ D_{pile}$) is of the correct order of magnitude compared to scour data from the literature ($d_{s,max} = 0.6$ to $1.2\ D_{pile}$), thereby confirming the validity of the experimental setup.

Caisson structure with monopile (GBS): The maximum scour depth is $d_{s,max} = 0.3\ D_{base}$ for $u_o/u_{cr} = 1.3$, which is in the middle of the literature data range ($d_{s,max} = 0.05$–$0.65\ D_{base}$). Whitehouse [11] measured much larger scour depths of 0.2 to 0.5 times the base foundation's diameter ($d_{s,max}/D_{base} = 0.2$–0.5) for high-current velocities ($u_o/u_{cr} = 4$ to 6). Tavouktsoglu [15] also measured much higher scour values of $d_{s,max}/D_{base} = 0.3$–0.65 for low-current velocities ($u_o/u_{cr} \cong 1.2$). Sarmiento et al. [16] measured a maximum scour depth along a caisson structure of about $d_{s,max} = 0.125\ D_{base}$ after 5 h in a movable bed ($d_{50} = 0.15$ mm); the scale model had a water depth of 1 m and a current velocity of 0.42 m/s ($u_o/u_{cr} \cong 2$).

Jacket structure: The absolute scour depth is much lower (factor 2) than that around the other two types of structures, see Table 2. The maximum scour depth near the leg of a jacket structure is $d_{s,max} = 2.5\ D_{leg}$ while that near a monopile is about $d_{s,max} = 1.1\ D_{pile}$. This means that the extra effect of the overall jacket structure on the scour near the legs is of the same order of magnitude. The scour depth with $d_{s,max} = 2.5\ D_{leg}$ measured during the present test ($d_{50} = 0.1$ mm) is higher than the scour depth with $d_{s,max} = 1.3$ to $1.75\ D_{pile}$,measured in the tests ($d_{50} = 0.19$ mm) of Welzel et al. (2019) [20], which may be related to the somewhat coarser sand used by Wenzel et al.

Figure 6. Scour near the pile's foundation structures.

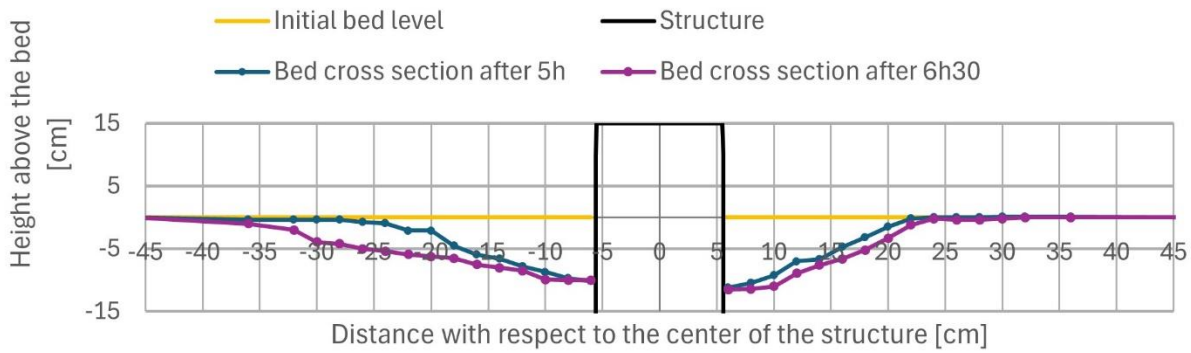

Figure 7. Scour near the monopile.

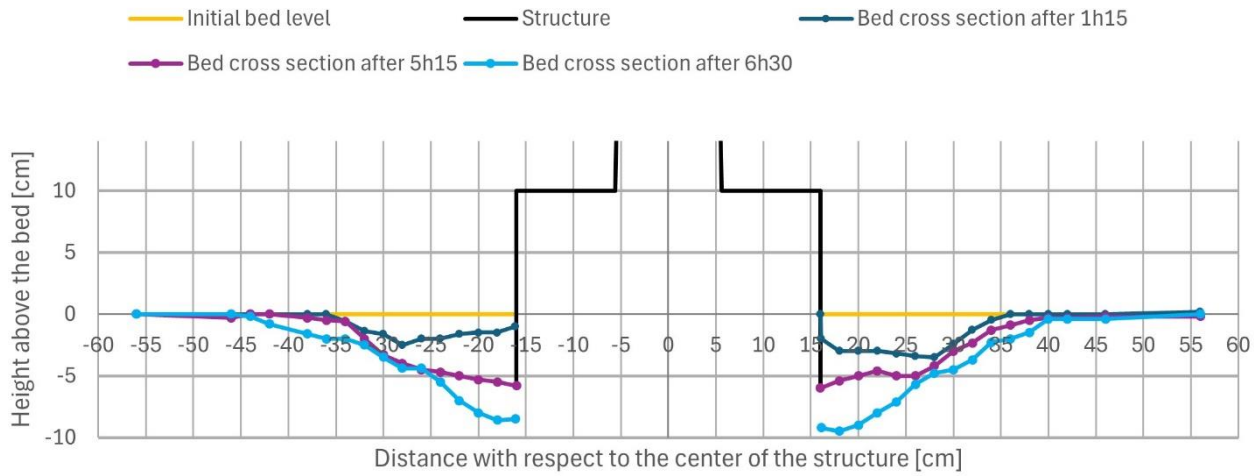

Figure 8. Scour near the caisson with a monopile (structure tipped over after 6.5 h, signifying end of test).

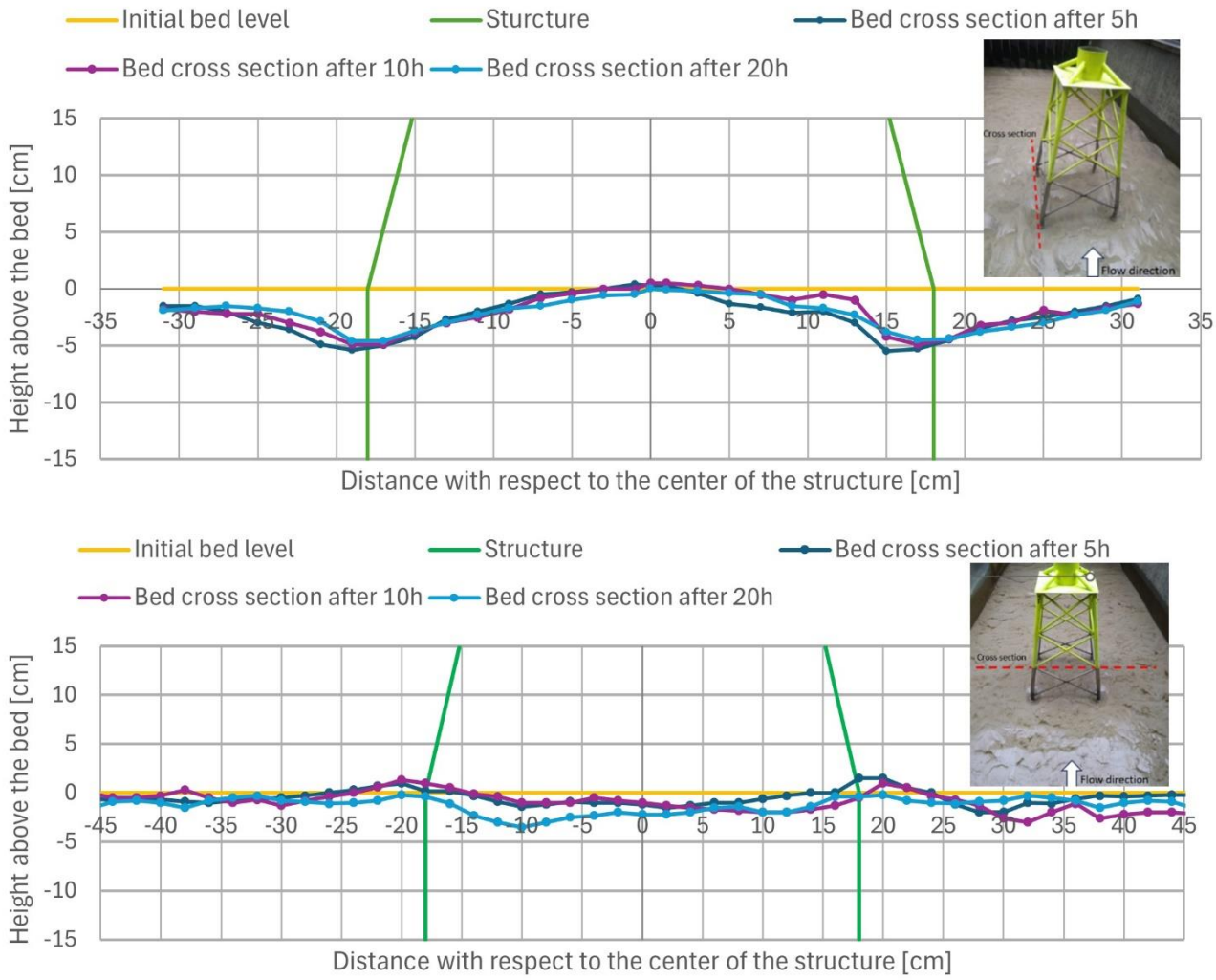

Figure 9. Scour near the legs of the jacket structure (2 cross-sections, see insets; green line is the pile's centre).

5. Scour Modelling and Results

5.1. General

Two scour models were recently developed and are presented herein: a semi-analytical 1D scour model (SEDSCOUR) for monopiles and jacket structures and a numerical 2DV model (SUSTIM2DV; [27,28]) for caisson-type structures. The SEDSCOUR model is a new model, described herein for the first time.

5.2. Scour near a Monopile and Jacket Structure: Description of the SEDSCOUR Model

5.2.1. General Schematization

The free scour hole/pit generated around a pile-type structure (without scour protection) is schematized into two separated scour pits on the upstream and downstream sides of the pile, as shown in Figure 10. The deepest scour pit is generated in the lee of the pile downstream of the highest peak tidal current velocity (assuming a slight velocity asymmetry; $u_{flood} > u_{ebb}$). Both scour holes are similar in shape. Herein, it is assumed that the flood current is dominant with the highest peak current velocity. Only the deepest scour hole (with scour depth d_s and length L_s) is considered (on the right in Figure 10). This scour pit consists of a deep scour pit near the pile and a shallow scour pit further away from the pile.

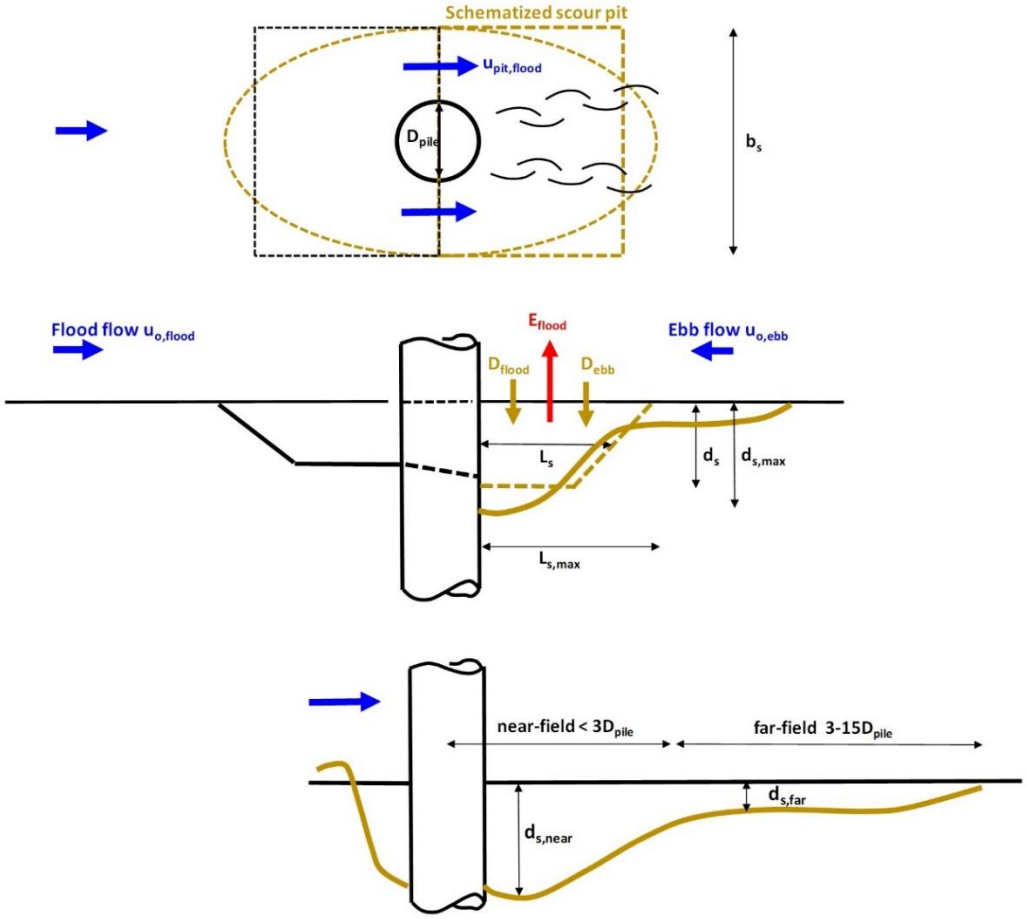

Figure 10. Plan view and cross-section of a scour pit due to tidal flow.

The tidal current is assumed to be perpendicular (normal) to the structure. Two tidal periods are considered: flood period of about 6 h with one flood-averaged and depth-averaged velocity u_{flood} and similarly an ebb period of about 6 h with one ebb-averaged and depth-averaged velocity u_{ebb}. Thus, each tidal phase (flood/ebb) is represented by one representative velocity. The variation in the flow velocity over the tidal cycle is not represented. The neap–spring variation in the velocities is represented by a sinusoidal variation based on input values. The scour pit erosion developing downstream of the pile over a tidal cycle of 12 h is the net result of the following tide-averaged sand transport processes:

- *flood*: the erosion of sand (E_{flood}) from the bed in the lee of the pile due to flow accelerations and increased turbulence levels and the deposition of sand (D_{flood}) from the incoming flood flow;
- *ebb*: the deposition of sand (D_{ebb}) from the incoming ebb flow (after reversal of the tidal current).

The SEDSCOUR model can also be used to compute the free scour downstream of a structure (obstacle) on the seabed such as a rock protection on a pipeline or a weir/sill in a riverbed, see Figure 11. The trapping of sand from the incoming sediment load (if present) is taken into account.

The scour process is assumed to be a two-dimensional process. Therefore, the scour width normal to the tidal current is set to $b_s = 1$ m (unit width). The mean scour length in the direction of the tidal current is assumed to be $L_s = \alpha_L h_s$ with h_s = the upstream structure or obstacle height and α_L = the input value.

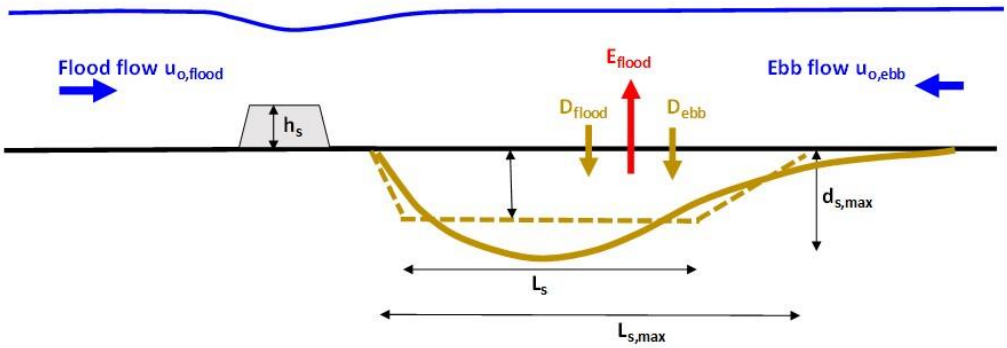

Figure 11. Scour downstream of a hard structure (obstacle) on the seabed.

5.2.2. General Model Equations

The deep part of a near-field scour pit is represented in the SEDSCOUR model as a rectangular box with the following dimensions: d_s = mean scour depth, b_s = mean scour width and L_s = mean scour length. The maximum scour depth is set to $d_{s,max} = \alpha_s d_s$ with α_s = the input value (range from 1.2 to 1.5). This parameter can be used as a safety factor. Using $\alpha_s = 1.5$ will give a conservative maximum scour depth.

The scour volume at time t is $V_{s,t} = d_{s,t}\, L_s\, b_s$

The net volume change per tide of 12 h is given as follows:

$$\Delta V_s = (E_{flood} - D_{flood} - D_{ebb}) \left(\frac{\Delta t_{tide}}{(1-p)\varrho_s}\right) \quad (1)$$

The scour volume at time t is

$$V_{s,t} = \sum \Delta V_s = \sum (E_{flood} - D_{flood} - D_{ebb}) \frac{\Delta t_{tide}}{(1-p)\rho_s} \quad (2)$$

The scour depth at time t is given as follows:

$$d_{s,t} = \frac{V_{s,t}}{b_s L_s} \quad (3)$$

The erosion (E) and deposition (D) parameters during each time step of $\Delta t_{tide} = 12$ h are:

$$E_{flood} = b_s[(q_{b,flood,pit} - q_{b,flood,o}) + \alpha_p (q_{s,flood,pit} - q_{s,flood,o})] \quad (4)$$

$$D_{flood} = b_s[\alpha_{D,b} q_{b,flood,o} + \alpha_{D,s} q_{s,flood,o}] \quad (5)$$

$$D_{ebb} = b_s[\alpha_{D,b} q_{b,ebb,o} + \alpha_{D,s} q_{s,ebb,o}] \quad (6)$$

with the parameters as follows:

$q_{b,flood,o}$ = the flood-averaged equilibrium of a bed load transport outside the pit based on undisturbed velocity $u_{flood,o}$;

$q_{s,flood,o}$ = the flood-averaged equilibrium of a suspended load transport outside the pit based on undisturbed $u_{flood,o}$;

$q_{b,ebb,o}$ = the ebb-averaged equilibrium of a bed load transport outside the pit based on undisturbed velocity $u_{ebb,o}$;

$q_{s,ebb,o}$ = the ebb-averaged equilibrium of a suspended load transport outside the pit based on undisturbed $u_{ebb,o}$;

$q_{b,flood,pit}$ = the flood-averaged equilibrium of a bed load transport in a scour pit area based on $u_{flood,pit}$;

$q_{s,flood,pit}$ = the flood-averaged equilibrium of a suspended load transport in a scour pit area on $u_{flood,pit}$;

α_P = the pickup coefficient of equilibrium for a suspended load transport ($\alpha_p < 1$ for suspended load); $\alpha_p = 1$ for bed load;
$\alpha_{D,b}$ = the trapping coefficient of equilibrium for a bed load transport ($\alpha_D = 1$ for bed load transport);
$\alpha_{D,s}$ = the trapping coefficient of equilibrium for a suspended load transport ($\alpha_D < 1$);
tanα = the downstream slope gradient of a near-field scour pit (1 to 7);
$\Delta t_{tide} = \alpha_{tide}\, T_{tide}$ = the effective time step of 1 tide; T_{tide} = the duration of a tidal cycle (≅12 h);
α_{tide} = the efficiency coefficient (velocities around slack tide are too small to cause substantial erosion; $\alpha_{tide} \cong 0.4$–0.6; this coefficient only affects the short term scour depth; it does not affect the long term scour depth).

It is noted that the pickup of sand particles in the scour pit is related to the excess sand transport rate (difference between sand transport in the pit and upstream sand transport); this ensures that the pickup is zero for a plane bed without a structure ($\alpha_u = 1$ and $r_o = 0$).

The equilibrium sand transport values are computed by the formulations proposed by Van Rijn [29–31], which depend on the depth-averaged velocity, the depth-averaged critical velocity for the initiation of motion, the water depth, the wave height (H_s), the wave period (T_p) and sediment parameters (d_{50}). The equilibrium transport rates are reduced if mud is present in the bed. The bed load transport equation [30] is

$$q_b = 0.015\, \gamma_b (1 - p_{mud})\, \rho_s\, u\, h\, M_e^{1.5} \left(\frac{d_{50}}{h}\right)^{1.2} \quad (7)$$

with

$$M_e = \frac{[u_e - (1+0.01 p_{mud}) u_{cr,o}]}{[(s-1) g d_{50}]^{0.5}};\ U_w = \frac{\pi H_s}{[T_p \sinh(kh)]};\ \mathrm{kh} = \mathrm{Y}^{0.5}[1 + 0.166\mathrm{Y} + 0.031\mathrm{Y}^2];\ Y = \frac{4.02h}{(T_p)^2}$$

Here, q_b = the bed-load transport (kg/m/s); h = the water depth; d_{50}= the particle size (m); p_{mud} = the percentage of mud/clay in the bed (0 to 30%); M_e = the mobility parameter; $u_e = u + \gamma U_w$ = the effective velocity with γ = 0.4 to 0.5 for irregular waves; u = the depth-averaged flow velocity; $s = \rho_s/\rho_w$ = the relative density; ρ_s = the sediment density; ρ_w = the fluid density; U_w = the peak orbital velocity (based on linear wave theory); H_s = the significant wave height; T_p = the peak wave period; $u_{cr,o}$ = the critical depth-averaged velocity for the initiation of motion of a pure sand bed; γ_b = the calibration factor (default = 1).

The suspended load transport equation [31] is

$$q_s = 0.012\, \gamma_s (1 - p_{mud})\, \varrho_s\, u\, h\, M_e^{2.4} \left(\frac{d_{50}}{h}\right) D_*^{-0.6} \quad (8)$$

where

$D_* = d_{50} \left[\frac{(s-1)g}{\nu^2}\right]^{0.333}$, q_s = the suspended load transport (kg/m/s), D_* = the dimensionless particle size, ν = the kinematic viscosity coefficient and γ_s = the calibration factor (default = 1).

The flood and ebb velocities outside ($u_{flood,o}$ and $u_{ebb,o}$) are the input values.

The depth-averaged flow velocity inside the scour pit/hole during the flood period is computed as

$$u_{flood,pit} = \alpha_u \alpha_r \left[\frac{h_{flood,o}}{h_{flood,o} + d_{s,t}}\right]^n u_{flood,o} \quad (9)$$

with

$\alpha_r = 1 + r_o \left(1 - \frac{\alpha_s d_s}{h_o}\right)^{0.5}$, α_u = the velocity increase factor related to the structure (range 1–1.3; input value),
n = the exponent (range 0.5–1; continuity gives n = 1; lower n-value gives higher velocity in pit and thus more pickup),

α_r= the turbulence factor related to structure, r_o= the initial turbulence effect close to structure (input), r_o decreases weakly for increasing scour depth (r_o = 0.1, 0.2, 0.3 for D_{pile}/h_o or $h_{structure}/h_o$ = 0.1, 0.3, 0.5; $r_{o,max}$ = 0.3) and α_s = the coefficient influencing the turbulence factor (≅ 0.3 reduction of turbulence in the scour pit; 0 = the turbulence factor is constant in the scour pit).

The trapping coefficient is given as follows:

$$\alpha_D = 1 - \exp\left(-\frac{A\, L_{eff}\, d_{s,t}}{h_{pit}^2}\right) \quad (10)$$

with

$$A = \gamma_{D1}\left[\frac{w_s}{u_{*,pit}}\right]\left[1 + \frac{2w_s}{u_{*,pit}}\right] \cong \gamma_{D2}\left[\frac{w_s}{u_{*,pit}}\right]^{1.5};\ u_{*,pit} = \frac{g^{0.5}u_{pit}}{C};\ C = 18\log\left(\frac{12h_{pit}}{k_s}\right);$$

where γ_{D1} = the calibration coefficient (input value 0.2 to 1; trapping α_D = 0 for γ_{D1} = 0; trapping α_D is higher for higher γ_{D1}) used in an earlier version of the model, γ_{D2} = the calibration coefficient (input value 0.1 to 0.7) used in latest model version, L_{eff} = the effective settling length, L_{eff} = 0.5 L_s + D_{pile} for flood and ebb flow, $d_{s,t}$ = the scour depth at time t; $h_{pit} = h_o + d_{s,t} +/- \eta_{max}$ = the water depth in a pit during flood/ebb, η_{max} = the tidal amplitude, h_o= the water depth to MSL, $u_{*,pit}$ = the bed-shear velocity inside the pit, C = Chézy's coefficient, k_s = the bed roughness height and w_s = the fall velocity suspended sand.

The pickup coefficient is given as follows:

$$\alpha_p = \alpha_{P,1}[1 - 0.01p_{mud}]\left[1 - \frac{d_{s,t}}{h_o}\right]\left[\frac{u_{*,pit}}{w_s}\right]^{0.3} \quad (11)$$

with $\alpha_{P,1}$ = calibration coefficient (0.5 to 1) and $u_{*,pit}$ = bed-shear velocity in pit.

The sand transport capacity (equilibrium transport) downstream of the structure in the flood period is much higher than the sand transport capacity upstream of the pile, and this is caused by the velocity increase and extra turbulence generation in the lee zone of the pile (vortex shedding). The actual sand transport in the lee zone close to the pile is somewhat smaller than the sand transport capacity due to the space lag effect (the growing effect of a suspended load due to upward transport processes). This effect is represented by a pickup coefficient (α_P < 1), which depends on the fall velocity (w_s) of the sand and the strength of the turbulence in the scour pit area ($u_{*,pit}$). The pickup coefficient gradually decreases for increasing scour depth because the pickup of sand is more difficult in a deep scour pit. The pickup coefficient is lower if mud is present in the bed.

Free scour around the pile without bed protection: The maximum scour depth is set to $d_{s,max} = \alpha_s d_s$ with α_s = 1.3 for laboratory cases (more triangular scour profile) and α_s = 1.2 for field cases. The scour width is assumed to be b_s = 3 D_{pile}. The mean scour length is assumed to be $L_s = \alpha_L d_s$ with an input value of α_L = 3 for laboratory scour pits and α_L = 7 for field scour pits. The maximum scour length is assumed to be $L_{s,max} = L_s + 0.5\, d_s/\tan\alpha$.

Edge scour near the pile with bed protection: In the case of a protected monopile, the scour processes develop at the edge of the scour protection and are similar to that of free scour, but the effects of velocity increase and extra turbulence production are much less (further away from the pile). A similar approach as for local scour can be used to compute the pickup and trapping of the sand particles.

Scour near piles of a jacket structure: In the case of a jacket-type structure, the main (tidal) flow will go through the open structure with slightly increased velocities (an overall increase of 15% to 20% depending on the blocking effect of the structure; locally, the increase may be higher, 20% to 30%, see Figure 3). The additional turbulence generated by the structure can be taken into account by a turbulence coefficient (r_o). The mean scour depth (d_s) follows from the net volume change per tide over the global scour area, where A_{global} = 1.5 b_{Jacket} x 1.5 L_{jacket}. The width (b_{jacket}) and the length (L_{jacket}) of the jacket structure

are the input parameters. The maximum scour depth ($d_{s,max}$) is set to $d_{s,max} = \alpha_s d_s$ with $\alpha_s \cong 1.2$.

5.3. Free Scour near the Monopile: The SEDSCOUR Model's Results (Cases A to D)

Two laboratory data sets of free scour (without bed protection) and two field cases are considered:

A. free scour around a monopile in flume experiments by Sheppard and Miller [32];
B. free scour around a monopile in flume experiments by Sheppard [33];
C. free scour around monopiles in the Q7 wind park (NL) in 2006–2007;
D. free scour around monopiles in the windpark Luchterduinen (NL) in 2013.

Case A: Sheppard and Miller [32] measured the scour depth around a monopile in a laboratory flume with a sand bed ($d_{50} = 0.27$ mm, fall velocity = 0.03 m/s, $u_{cr} = 0.27$ m/s, porosity = 0.4 and sediment density = 2650 kg/m^3). The water depth was about 0.42 m. The pile diameter was 0.152 m. The approach current velocity was varied in the range of 0.17 to 1.64 m/s. The test with a velocity of 0.17 m/s is a clear-water scour test (no sediment load in upstream current); the other tests are live-bed scour tests with the recirculation of the sediment load. The basic data and model input coefficients are given in Table 3. The velocity increase coefficient, which is a calibration coefficient, is set to $\alpha_u = 1.4$ for all cases; the turbulence coefficient is in the range of $r_o = 0.3$ to 0.4. The pickup and trapping coefficients are the same for all cases ($\alpha_P = 1$ and $\alpha_D = 0.5$). The calibration coefficient of the sand transport outside and inside the scour hole is set to one (column 5 of Table 3). Test 1 is a clear-bed scour as the upstream depth-averaged flow velocity is smaller than the critical velocity ($u_o/u_{cr} < 1$). The bed roughness (column 6 of Table 3) is estimated based on personal experience, assuming small-scale ripples with $k_s = 0.03$ m for $u < 0.7$ m/s and gradually washed-out ripples to a flat mobile bed with $k_s = 0.003$ m (3 mm) for higher velocities. The measured and computed dimensionless scour depths ($d_{s,max}/D_{pile}$) are shown on the vertical axis of Figure 12. The value $\alpha_s = d_{s,max}/d_s$ is set to 1.3 for all tests (maximum scour is assumed to be 1.3 times the mean scour depth). The horizontal axis refers to the ratio of the current velocity and critical velocity for the initiation of motion (u/u_{cr}). The computed values of the maximum scour depth show rather good agreement (about 10% too small) with measured values for all live-bed scour test results, but the computed value is too high (20%) for the clear-water scour test result.

The time scale is 200 h for the clear-water scour tests and less than 1 h for most of the live-bed scour tests.

Figure 12 also shows the maximum scour depth data of the monopile test of the present tests (square symbol; data from Table 2). The results are in good agreement with the other data.

Case B: Sheppard [33] measured the scour around a monopile in a long, wide flume with a water depth of 1.22 m above a short sand bed with $d_{50} = 0.22$ mm, fall velocity $\cong$ 0.025 m/s, critical velocity $u_{cr} \cong 0.3$ m/s, bed porosity = 0.3 and sediment density = 2650 kg/m^3. The current velocity was 0.31 m/s. The model's settings are given in Table 4. The settings of the α_u and α_P coefficients which are used as calibration coefficients are slightly different (compared to Case A) to achieve the best agreement with the measured values.

Figure 13 shows the measured and computed maximum scour depths as a function of time. The computed maximum equilibrium scour depth is about 0.43 m, which is somewhat higher (15%) than the measured values of 0.37 m ($\cong 1.2\ D_{pile}$). The time scale of the measured equilibrium scour depth is about 50 h, which is much shorter than that of the computed value of 150 to 200 h. Most likely, the strong effect of the near-bed horseshoe-type vortices is not sufficiently well represented in the SEDSCOUR model.

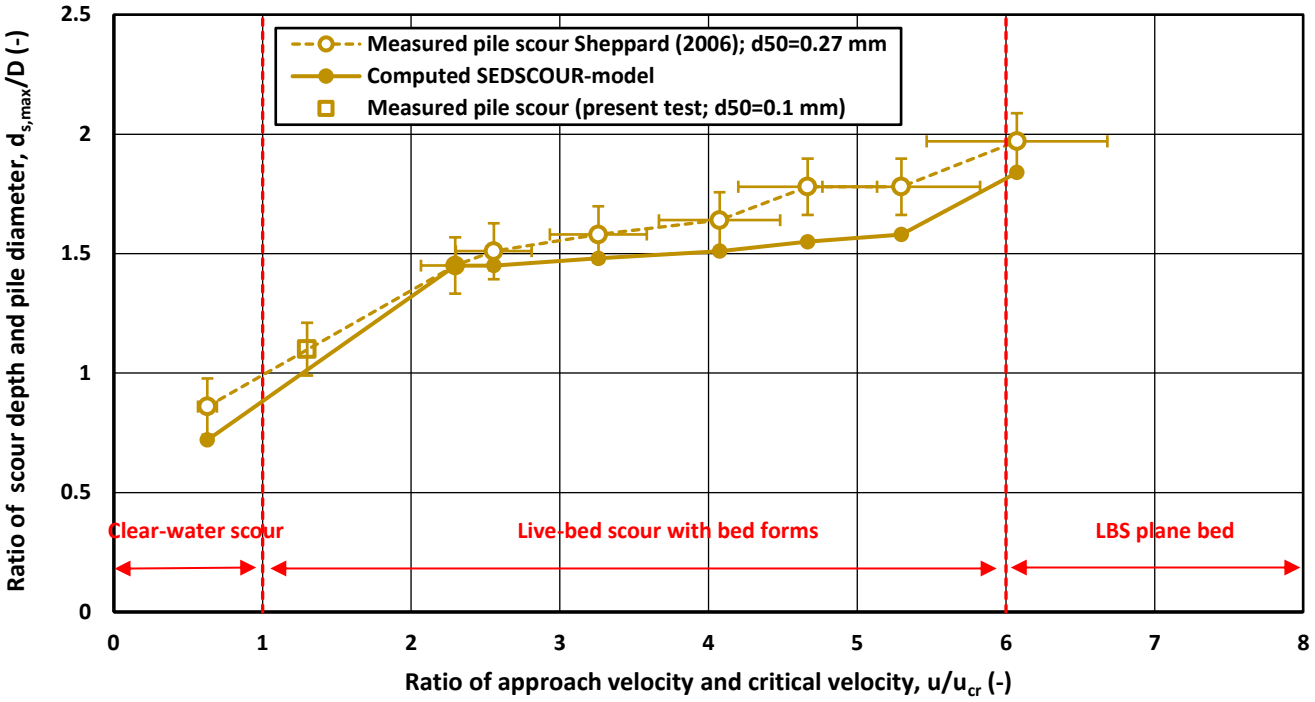

Figure 12. Case A: scour depth as a function of current velocity; tests by Sheppard and Miller [28].

Table 3. Case A: measured and computed scour depths and model coefficients; tests by Sheppard–Miller [28].

Test	Current u_o (m/s)	Measured scour depth $d_{s,max}$ (m)	Computed scour depth $d_{s,max}$ (m)	Bed and suspended load coefficients γ_b, γ_s (-)	Bed roughness k_s (m)	Turbulence coefficient r_o (-)	Velocity increase coefficient α_u (-)	Pickup coefficient α_P (-)	Trapping coefficient α_D (-)	Scour length coefficient α_L (-)	Time scale T_{scour} (hours)
1	0.17	0.13	0.1	default = 1	0.03	0.4	1.4	1	0.5	3	200
2	0.62	0.22	0.21	default = 1	0.03	0.3	1.4	1	0.5	3	2
8	0.69	0.23	0.22	default = 1	0.03	0.3	1.4	1	0.5	3	1
3	0.88	0.24	0.23	default = 1	0.02	0.3	1.4	1	0.5	3	<1
4	1.10	0.25	0.255	default = 1	0.01	0.3	1.4	1	0.5	3	<1
5A	1.26	0.27	0.26	default = 1	0.005	0.3	1.4	1	0.5	3	<1
5B	1.43	0.27	0.275	default = 1	0.003	0.3	1.4	1	0.5	3	<1
6	1.64	0.3	0.3	default = 1	0.003	0.4	1.4	1	0.5	3	<1

Table 4. Case B: measured and computed scour depths and model coefficients; test by Sheppard [29].

Test	Current u_o (m/s)	Measured scour depth $d_{s,max}$ (m)	Computed scour depth $d_{s,max}$ (m)	Bed and suspended load coefficients γ_b, γ_s (-)	Bed roughness k_s (m)	Turbulence coefficient r_o (-)	Velocity increase coefficient α_u (-)	Pickup coefficient α_P (-)	Trapping coefficient α_D (-)	Scour length coefficient α_L (-)	Time scale T_{scour} (hours)
12	0.31	0.37	0.43	default	0.03	0.2	1.2	0.7	0.5	3	200

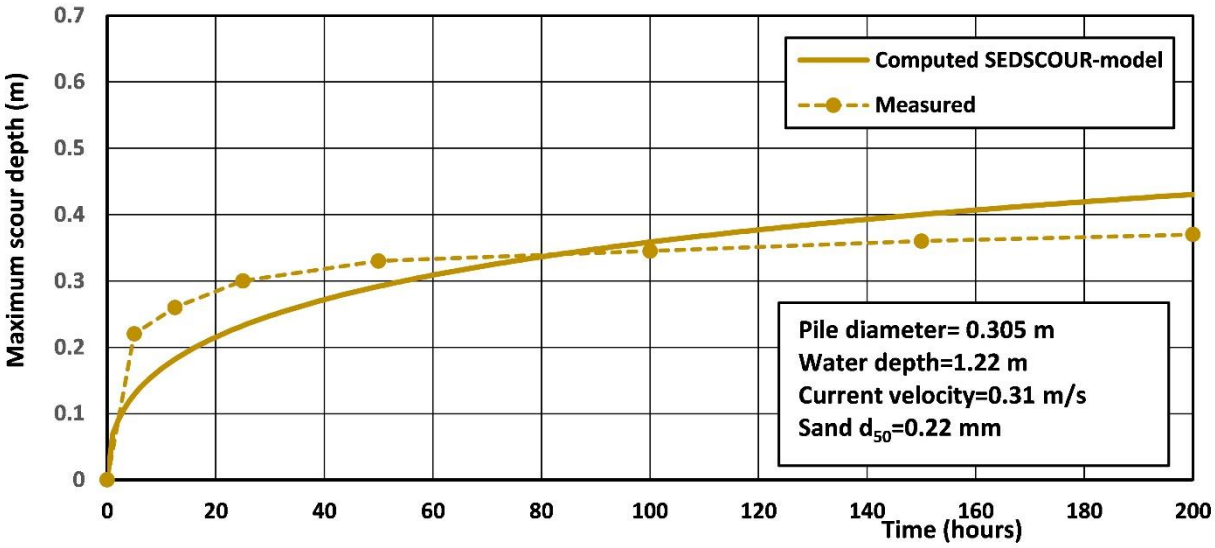

Figure 13. Case B; measured and computed scour depths as a function of time; test by Sheppard (2003), [33].

Case C: The offshore wind park Q7 Princess Amalia was built in 2006/2007 at about 20 km off the Dutch coast. The water depths were between 20 and 25 m. The bed consisted of medium-fine sand (0.2 to 0.3 mm). The monopiles (diameter of 4.0 m) were exposed to waves and currents for several months without scour protection. The tidal range was about 2 m. The main direction of the tidal current was SSW-NNE. The maximum tidal current during a spring tide was about 0.9 m/s (depth-averaged). The driving hydrodynamic signal is a (modulated) sine wave varying over the neap–spring cycle (14 days) based on the measured values. The basic data are given by [9].

The measured maximum scour depths of 29 monopiles (without scour protection) were in the range of 1.5 to 4.5 m (3 ± 1.5 m), see also Figure 14. The variation is most likely related to variations in the hydrodynamic conditions, which are not exactly the same among the piles. The scour extent (radius of longest axis) was about 20 to 30 m. The shape of the scour hole was oval with a length ratio of 1.8 between the main axis (averaged radius 27 m) and the short axis (average radius 15 m). The side slopes of the scour pit were rather mild (1 to 10), which is very different from the steep side slopes often found in laboratory experiments (1 to 2 or 1 to 3). Measured and computed scour depth are shown in Figure 14. The measured values are those of Pile 48 [9]. The model input data are given in Table 5. The neap–spring tidal cycle is represented by a sinusoidal function with a maximum (tide-averaged) velocity of 0.7 m/s during spring tide and 0.3 m/s during neap tide. The wave height is set to a value of 1 m (no storms). The agreement between measured and computed scour depths is rather good on average, but the variability of the measured data is rather large.

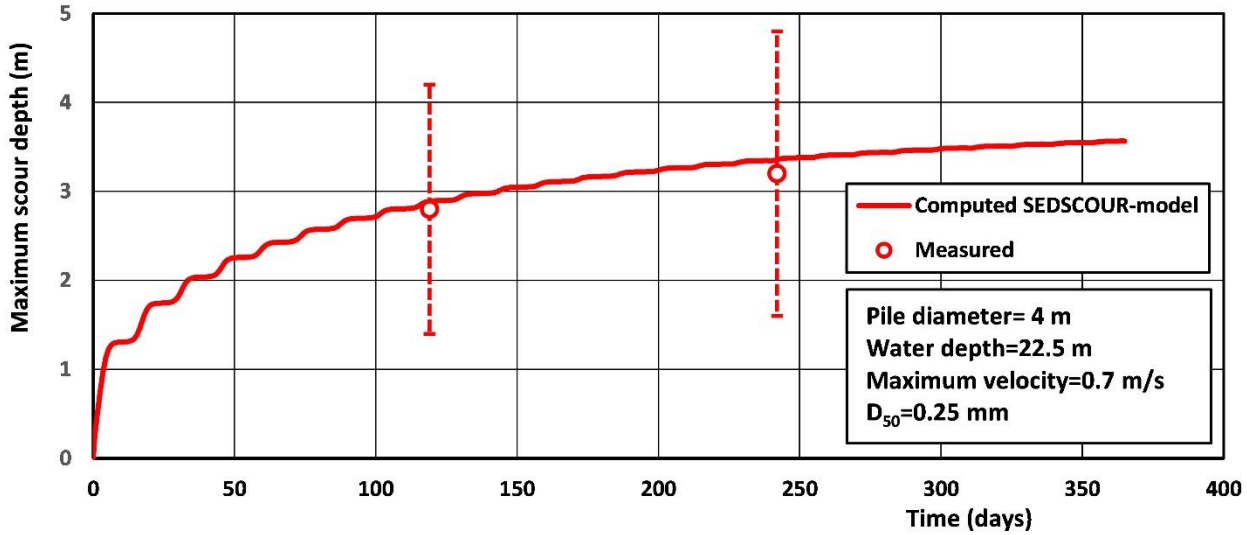

Figure 14. Case C: measured and computed free scour depths as function of time; Q7 windpark (NL).

Table 5. Model input data of field cases [9].

Parameter	Wind Park Q7 North Sea (NL) Case C	Luchterduinen North Sea (NL) Case D	Global and Free Scour L9 Jacket North Sea (NL) Case E
Pile diameter (m)	4	5	1.2
Water depth to Mean Sea level (m)	22.5	23	22.5
Maximum tidal velocity in spring (m/s)	0.7	0.7	0.7
Maximum tidal velocity in neap (m/s)	0.3	0.3	0.3
Tidal range (m)	2	2	2
Significant wave height H_s (m) and peak period T_p (s)	1; 7	1; 7; 3 storms	1; 7
Sand diameter d_{50} (mm)	0.25	0.25	0.25
Percentage fines/mud < 63 μm (%)	5	5	5
Fall velocity sand w_s (m/s)	0.03	0.03	0.03
Critical velocity u_{cr} (m/s)	0.4	0.4	0.4
Bed roughness k_s (m)	0.03	0.03	0.05
Velocity increase coefficient α_u (-)	1.3	1.3	1.3
Turbulence coefficient r_o (-)	0.3	0.3	0.3
Pickup coefficient α_P (-)	0.7	1.2	1
Trapping coefficient suspended sand transport α_D (-)	0.7	0.7	0.5
Pit length coefficient α_L (-)	10	10	10
Calibration factor bed and suspended load γ_b, γ_s (-)	1	1	1

Case D: The wind park Luchterduinen (NL) consisting of 43 monopile foundation structures (D_{pile} = 5 m) was built in 2013 at about 23 km off Holland's coast between the beach villages of Noordwijk and Zandvoort, The Netherlands [34]. The local bed of medium-fine sand (0.2 to 0.3 mm) was about 23 m below MSL. The tidal range was about 2 m. The maximum flood current to NNW was about 0.7 to 0.9 m/s; the maximum ebb current to the SSW was about 0.5 to 0.6 m/s. Wave heights in the winter period were between 2 and 6 m. Two monopile foundations were installed without scour protection to monitor the free scour development. Figure 15 shows the measured scour depth of the unprotected

monopile as a function of time. The scour depth gradually increases from about 3 m on 1 October 2013 to about 4.5 m on 1 November 2014 (over period of about 400 days). The measured scour depth shows a pronounced dip around the period with storm waves, which is most likely caused by the backfilling process in the deep scour due to sand coming from upstream (outside). The scour pit extent was of the order of 25 m (≅5 D_{pile}). Computed scour depths are also shown in Figure 15. The model input data are given in Table 5. The neap–spring tidal cycle is represented by a sinusoidal function with a maximum (tide-averaged) velocity of 0.7 m/s during spring tide and 0.3 m/s during neap tide (modulated sine function with a period of 14 days). The wave height is set to a value of 1 m for daily conditions; three storms with waves gradually increasing from 1 to 6 m and decreasing from 6 to 1 m over a period of 3 days are included (superimposed on the tidal velocities of the neap–spring cycle at the proper time moments based on measured data). The overall agreement between measured and computed scour depths is rather good. The model computes small (underestimated) dips in the scour depth values. This can be improved by using a higher trapping coefficient (more research is required).

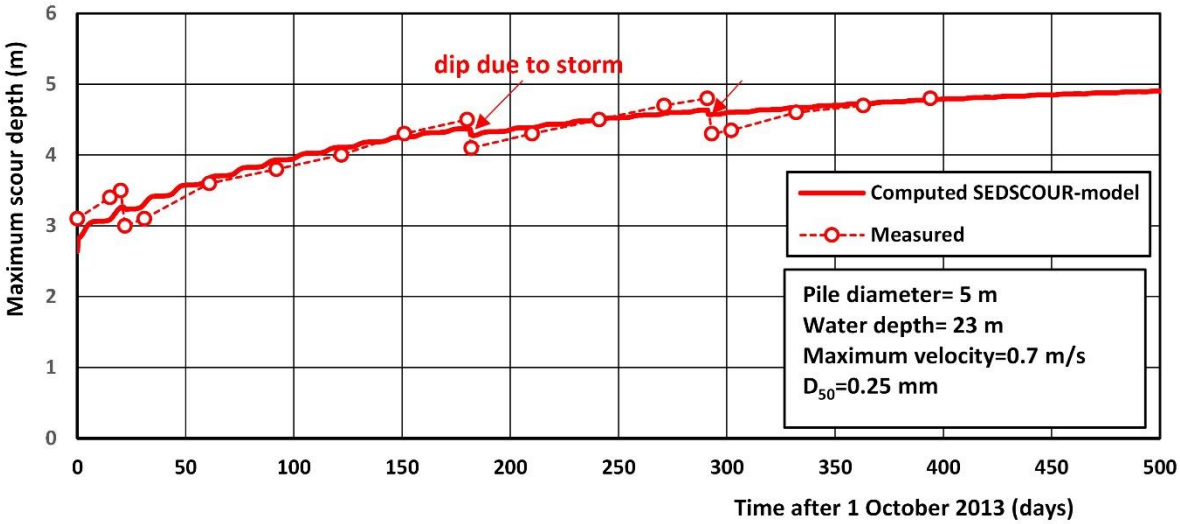

Figure 15. Case D: measured and computed free scour depths as a function of time; Luchterduinen wind park (NL).

5.4. Free Scour near Jacket Structure: The SEDSCOUR Model's Results (Case E)

The free scour near the legs of a jacket structure and the overall global scour can also be predicted using the SEDSCOUR model. One field case is considered herein: Case E, which is a jacket structure with four legs installed without scour protection at location L9 in the North Sea, about 30 km north of the island of Texel (The Netherlands) in the summer of 1997 [17]. The bed level was about 24 m below LAT (about 27 below MSL). The jacket structure has four legs with diameter D_J = 1.1 m and a spacing of 20 m and 17 m. The diameter of the piles in the seabed is D_{pile} = 1.2 m. The bed consisted of fine sand (0.2 to 0.3 mm). Typical depth-averaged peak flow velocities were 0.5 m/s during spring tide and 0.35 m/s during neap tides. The maximum measured wave height and current velocity since installation in 1997 was H_s = 7.8 m, T_p = 9.8 s and u = 1.0 m/s. The measured maximum global scour depths were in the range of 1.5 to 3 m. The extent of the global scour hole was of the order of 50 m (≅40 D_{pile}) in all directions. The maximum scour around the foundation pile B2 was found to be about 5 m consisting of global scour and local pile scour. Assuming a global scour depth of 2.5 m (50% based on the data of Table 2), the maximum local pile scour is about 2.5 m (about 2 D_{pile}). The model input data are given in Table 5. The width and length of the jacket foundation structure are 20 m (input). The

computed scour depths are shown in Figure 16. The neap–spring tidal cycle is represented by a sinusoidal function with a maximum (tide-averaged) velocity of 0.7 m/s during spring tide and 0.3 m/s during neap tide. The wave height is set to a value of 1 m (no storms). The maximum computed global scour depth is of the order of 2 m after about 1.5 years. The local maximum scour depth near the pile (D_{pile} = 1.2 m) of the structure is about 3 m after 1.5 years. The total maximum computed scour depth is 2 + 3=5 m after 1.5 years. The total maximum scour observed near leg B2 is about 5 m after 3 years (pile scour ≅2.5 m and global scour ≅2.5 m). Hence, computed and measured values are in good agreement, see Figure 16.

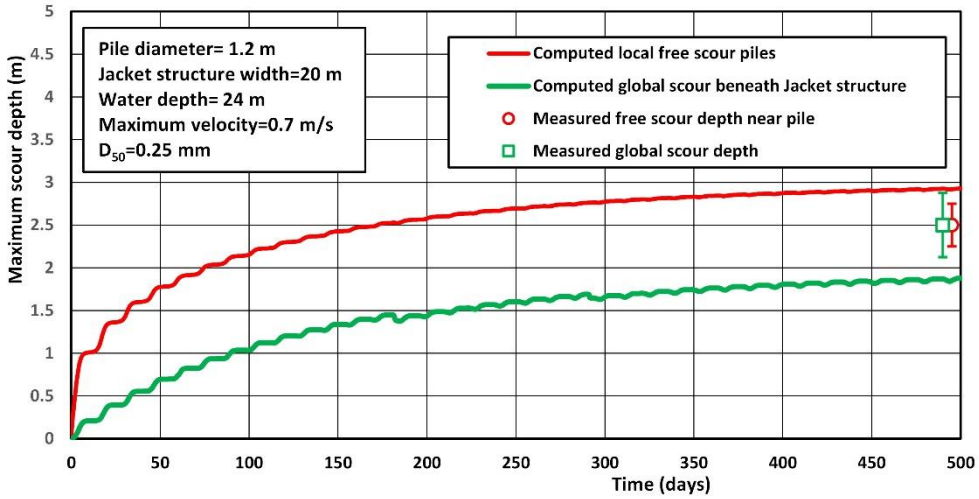

Figure 16. Case E: computed scour depth as a function of time; Jacket structure L9, North Sea (NL).

5.5. Free Scour Along a Caisson Type Structure: The SUSTIM2DV Model's Results (Case F)

5.5.1. General

This example (Case F) considers the scour near a caisson-type structure with a diameter of 40 m and a height of 8.8 m in a water depth of about 35 m (to mean sea level). The monopile on top of the structure has a diameter of 11 m. The prediction of scour around the flanks of a large-scale caisson-type structure with a monopile on top of it essentially requires the use of a 3D morpho-dynamic model. Given the complexity and long run times of 3D models, a more pragmatic approach is used herein, based on a combination of a depth-averaged flow model (DELFT3D) and a two-dimensional vertical morpho-dynamic model (SUSTIM2DV [27,28]). This latter model can simulate the scour processes and the long-term bed development in a stream tube along the perimeter of the caisson structure. The stream tube width is derived from the 2DH model's results and is assumed to be constant in time.

5.5.2. Computed Flow Field of the DELFT3D Model

The DELFT3D model was operated in 2DH (1 layer) and 3D mode (eight equidistant layers of 4.5 m) to compute the flow field. A rectangular computational grid was constructed. The grid was nonuniform in both directions, with a gradual transition in grid cell size, in order to obtain the highest resolution close to the structure. In total, the grid comprises 347 cells in the streamwise direction and 107 cells in the spanwise direction. Accordingly, the grid spans approximately 1600 m and 800 m in either direction, respectively. Close to the structure, the cells have a resolution of 2 m in both directions.

To obtain a unidirectional current in the far-field part of the spatial domain, an open boundary was defined at the upstream boundary where a constant current velocity is prescribed. At the downstream end of the spatial domain, another open boundary was

defined where a constant water level was prescribed. At the lateral closed boundaries, a free-slip condition was applied, implying that the tangential shear stress is zero. Basic input parameters are as follows: Chézy's coefficient C = 60 $m^{0.5}/s$, a k-epsilon model for vertical turbulent viscosity and horizontal large eddy simulation (HLES) for horizontal turbulent viscosity, time step = 0.3 s. Figure 17 shows the depth-averaged flow velocity vectors for the 2DH and 3D mode. The depth-averaged current velocities are quite similar, except for the wake region. Both model results show large-scale eddy circulations, but the vortex streets in the 3D model are less well developed, which may be caused by the limited number of layers (only eight layers). Most likely, much more vertical layers (resolution) are required for accurate results. Additional research is needed to determine the optimum number of layers for accurate 3D model results. The general mean flow of the 2DH and 3D runs are reasonably similar. Figure 18 shows the flow velocity vectors in the near-bottom layer of the 3D run. The approach velocity in the near-bottom layer is about 0.15 m/s. The distribution of the relative depth-averaged current velocity vectors along the flank of the base structure based on the 2DH and 3D model runs is shown in the left side of Figure 19. The acceleration computed using the 2DH and 3D models is very similar, based on the depth-averaged current velocity. The maximum increase in the depth-averaged velocity is about 20% with respect to the approach current velocity. The right side of Figure 19 shows the computed relative velocity vector magnitude close to the bottom along the perimeter of the foundation structure based on the 3D model run (see inset sketch). Most apparent is that the computed acceleration at this height along the flank is significantly stronger ($u_{nearbed,flank} \cong 1.8\ u_{nearbed,\ approach}$).

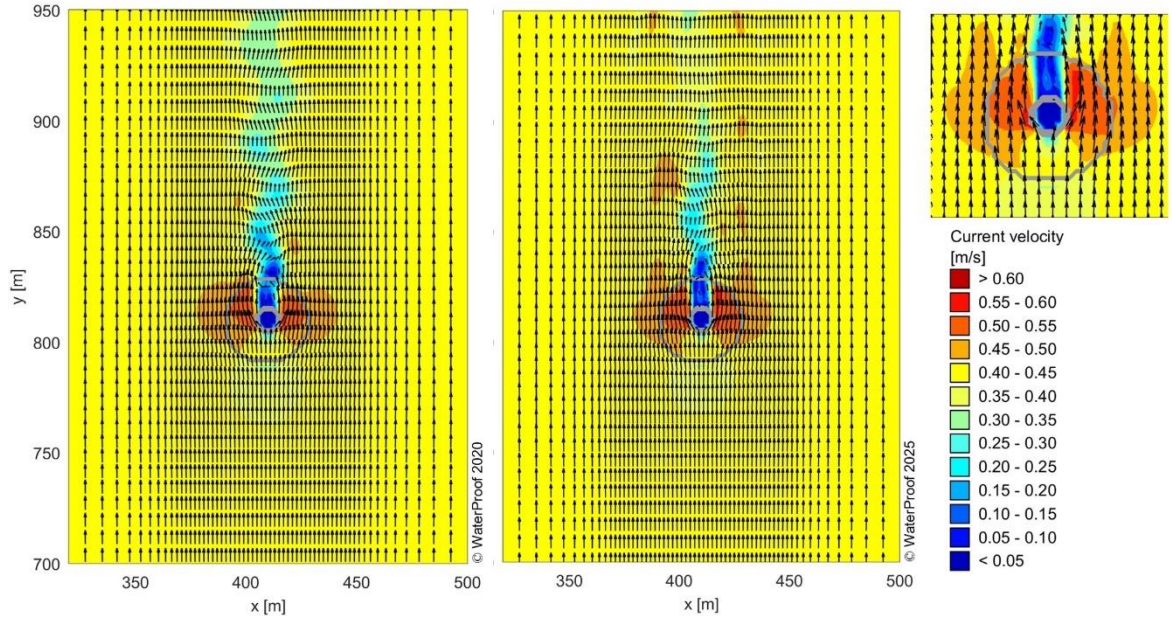

Figure 17. Case F: depth-averaged flow field based on the 2DH mode (**left**) and 3D mode (**right**); depth-averaged approach velocity $u_o = 0.42$ m/s.

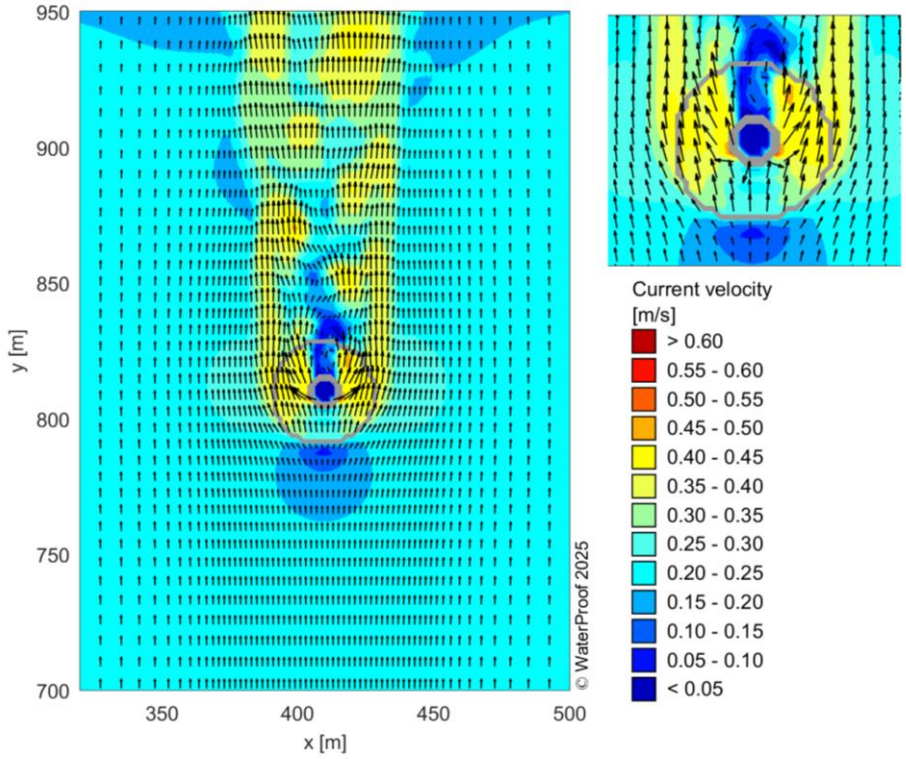

Figure 18. Case F: flow field in the near-bottom layer of the 3D model run; u_o = 0.42 m/s.

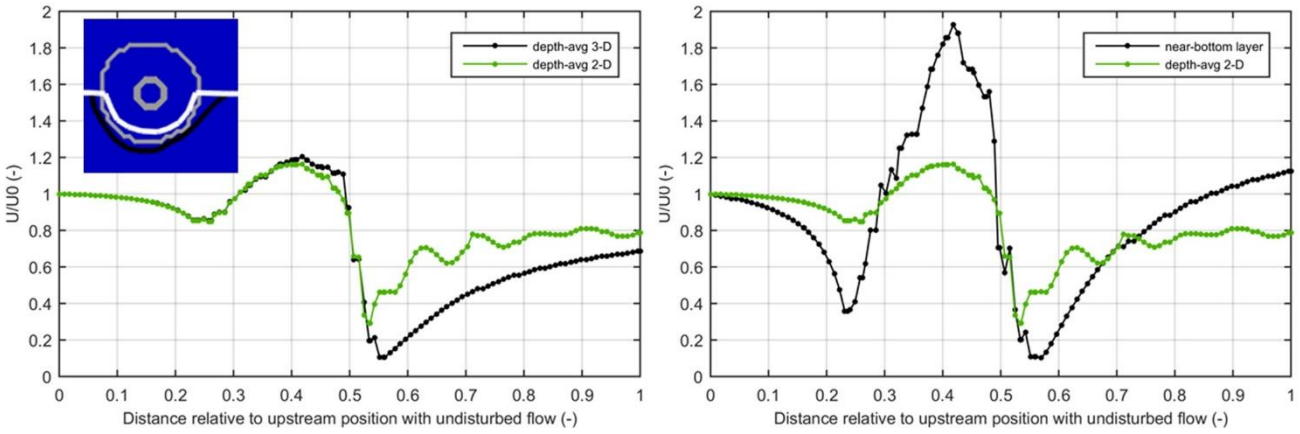

Figure 19. Left: depth-averaged flow velocity of the 2DH and 3D model runs along the structure (see inset sketch); **Right**: flow velocity of 2DH along the structure and 3D in the bottom layer along the structure (u_o = 0.42 m/s for depth-averaged flow; u_o = 0.15 m/s near-bottom for 3D model)

5.5.3. Computed Erosion in a Stream Tube Along the Flank of Caisson

As an example of the SUSTIM2DV model, the sand transport in accelerating and decelerating flows along a caisson structure (diameter D = 40 m and height h = 10 m; effective water depth = 10 m) with a monopile on top of it is considered, see Figure 20. Thus, the caisson occupies the whole water depth in the SUSTIM model run. The maximum flow velocity along the flank is assumed to be 1.7 times the upstream approach velocity ($u_{flank} \cong 1.7\ u_o$), which is slightly smaller than the computed value (1.8 u_o) of the 3D results, see the right side of Figure 19. The minimum width of the stream tube at the flank is set to 0.6 of the width at the entrance ($b_{minimum} \cong 0.6\ b_o$). The width along the stream tube along the centreline is derived (schematically) from the computed values of the DELFT-flow model. The basic input data are as follows: water depth upstream of trench (10 m to MSL), tidal

current with semi-diurnal amplitude of 1 m and peak current of 1 and 0.7 m/s (no phase difference between vertical and horizontal tides, constant semi-diurnal tidal sine function and no modulation of the neap–spring cycle), sand with d_{50} = 0.4 mm (critical bed-shear stress computed from Shields' curve in the model), computation period = 90 days, time step = 8 s and NZ = 25 = the number of vertical points over the depth.

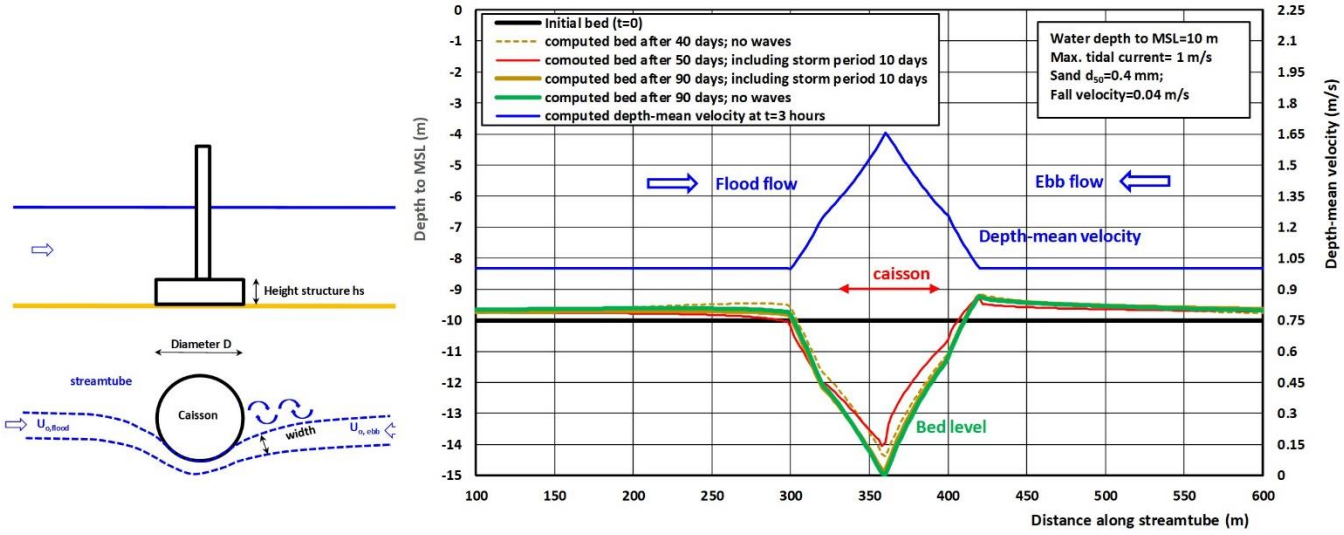

Figure 20. Case F: flow and scour around caisson (diameter = 40 m; height = 10 m; seabed = 0.4 mm sand).

The computed scour results for a peak velocity of 1 m/s are shown in Figure 20. The maximum scour depth is about 4.5 m after 40 days (no waves). The maximum scour depth decreases to 4 m after 50 days due to deposition during the storm period of 10 days (H_s = 3 and 4 m between t = 40 to 50 days). The maximum scour depth increases to 5 m after 90 days due to current (no waves between t = 50 and 90 days). Often, it is necessary to install scour protection. The structure may also be placed in a dredged pit with a depth of 2 to 3 m to reduce the scour depth. Steel skirts can be attached to the foundation's structure to slow down the time until the undermining of the caisson structure. Additionally, bed protection should be placed around the structure in conditions with strong flows.

Figure 21 shows the computed scour hole over 90 days for a lower peak tidal flow velocity of 0.7 m/s (instead of 1 m/s), resulting in a lower sand transport value during peak tidal flow conditions. The maximum scour depth is about 1.8 m after 40 days (tidal flow without waves), which increases to about 2.6 m after 50 days for tidal flow and a storm period of 10 days (t = 40 to 50 days) with H_s between 3 and 4 m. The maximum scour depth increases to about 2.8 m after 90 days due to tidal current (no waves between t = 50 and 90 days). The maximum scour depth after 90 days is slightly smaller (2.5 m) in conditions without a storm period. The scour on the left slope is lower, and the deposition on the left side is somewhat higher.

Figure 22 shows the effect of a storm period of 10 days with H_s between 3 and 4 m on the deposition in the deep scour hole around the base caisson structure with a maximum depth of 5 m in a sand bed of d_{50} = 0.25 mm (critical bed-shear stress according to Shields' curve). In this case, the initial bed represents a scour hole with a maximum depth of 5 m. The flow velocity in the deepest part of the scour hole increases due to flow contraction around the structure, but the flow velocity decreases due to flow expansion (larger water depth in scour hole). Overall, the flow velocity increases slightly (10% to 15%). The maximum upstream depth-mean velocity at t = 3 h (peak tidal flow) is about 0.7 m/s, which increases slightly to 0.8 m/s. The deposition of sand occurs in the storm period, mostly at the right slope due to higher sand transport during ebb flow when the water depth is

smallest. Erosion occurs on the left slope. Thus, deposition prevails in a scour hole during a storm period (Figures 20 and 22). Overall, the computed maximum scour depth near the base caisson structure is in the range of 3 to 5 m, which is of the right order of magnitude based on the physical model study by Sarmiento et al. (2024) [16].

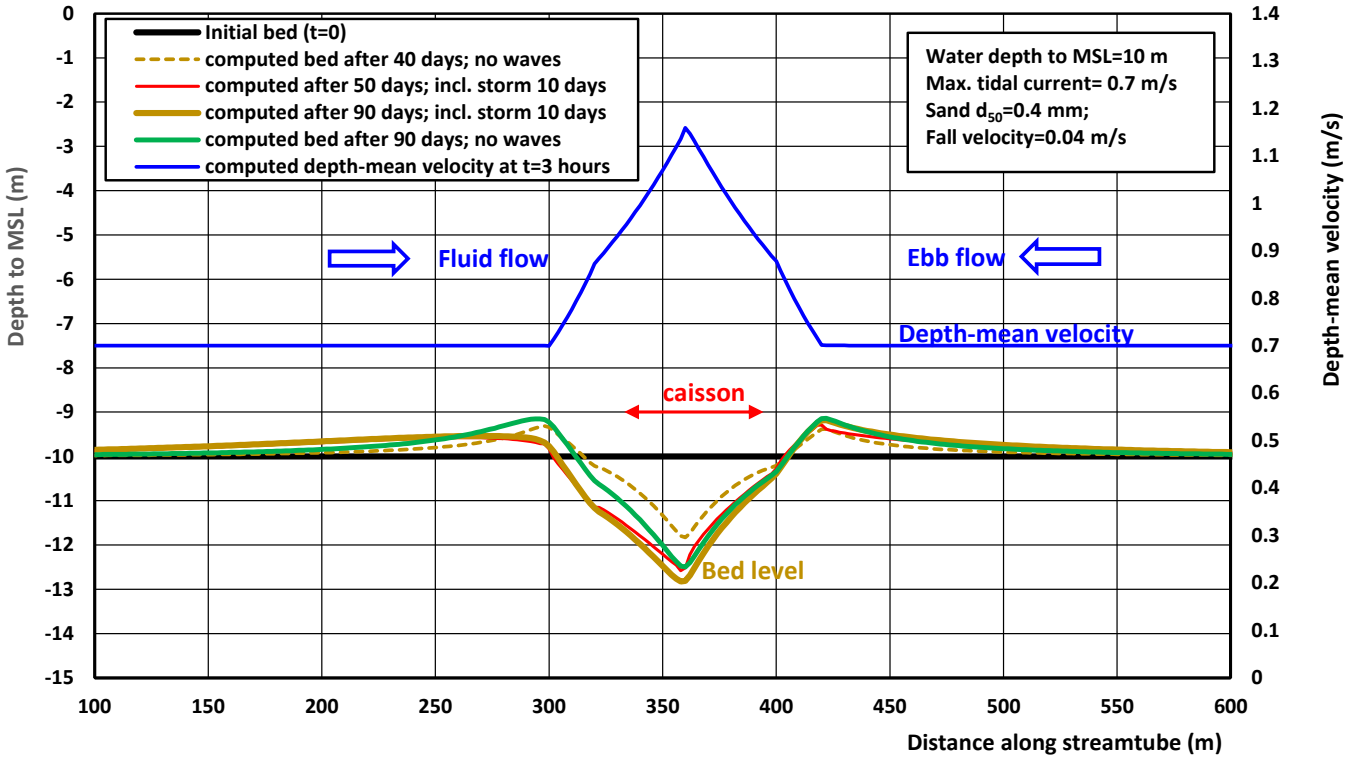

Figure 21. Case F: flow velocity and scour along the stream tube; maximum velocity= 0.7 m/s; d_{50} = 0.4 mm.

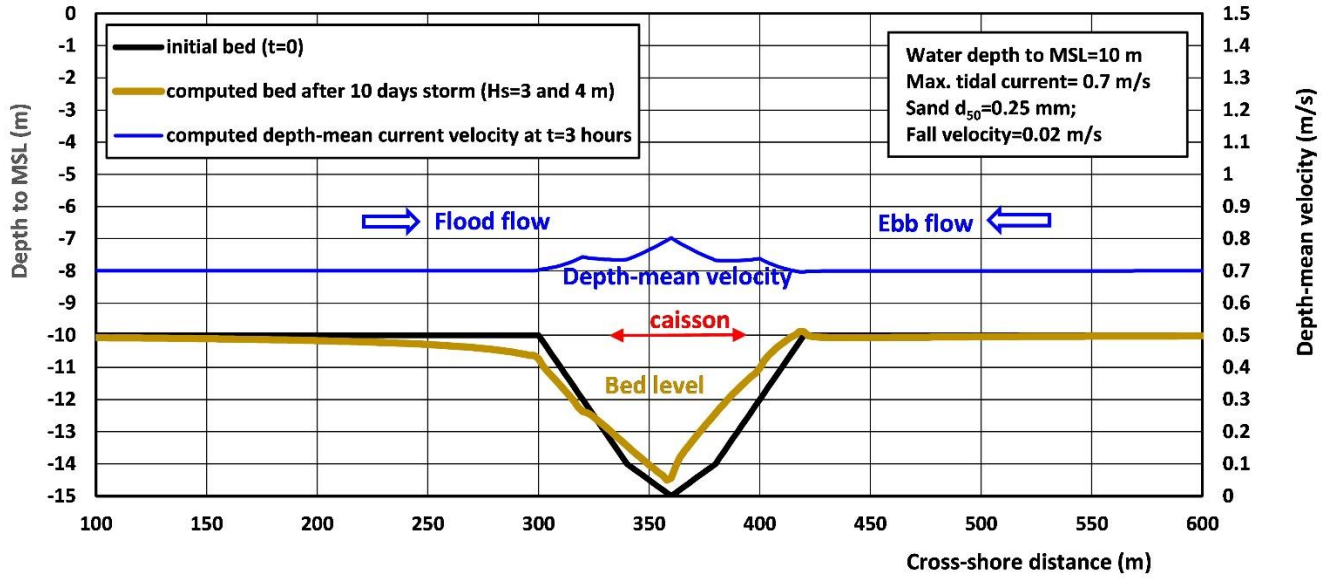

Figure 22. Case F: flow velocity and scour along the stream tube; maximum upstream velocity= 0.7 m/s; d_{50} = 0.25 mm.

6. Summary and Conclusions

The scour near various offshore structures (monopile, caisson foundation and jacket structure) were studied by performing laboratory tests in a wide flume and numerical model runs with a semi-empirical model (SEDSCOUR) and a sophisticated 2DV model (SUSTIM2DV). Measured and computed results were also compared to scour data from the international literature. The laboratory test results show that the maximum free scour depth ($d_{s,max}$) around a monopile without bed protection is slightly higher than the pile diameter ($d_{s,max} = 1.1\ D_{pile}$) for a mobility number of $u_o/u_{cr} = 1.3$ (weak to moderate flows). The scour depth may be significantly higher for strong flow conditions.

The maximum scour depth along the flank of a circular caisson foundation structure is found to be related to the base diameter of the structure ($d_{s,max} \cong 0.25\ D_{base}$). The skirt under the caisson structure should be relatively long; otherwise, it may easily be undermined due to erosion causing the tip over of the total structure.

The maximum scour consisting of pile scour and global scour around an open jacket structure standing on four piles is found to be much lower than the scour near the other structures (monopile and caisson).

The main cause of the scour near these types of structures is the increase in the velocity along the flanks of the structure (pile and caisson). Detailed velocity measurements showed a significant increase in the depth-averaged velocity, up to 40%. The increase in the near-bed velocity may be even higher (up to 70%) based on the DELFT3D model runs, resulting in a strong increase in the pickup and transport of sediments and associated erosion.

The measured scour depth values of the physical model tests with the monopile and the open jacket structure of this study are in reasonable agreement with other scour data from the literature. The dimensionless scour parameters are also in reasonable agreement with measured field scour data of monopiles and jacket structures. Hence, the many available scour data sets are sufficiently reliable to be used for scour predictions of similar structures. It is more difficult to evaluate the measured scour data of a circular caisson foundation. The measured maximum scour depth along the flank of the caisson of the present laboratory tests is much higher (factor 2) than that measured by Sarmiento et al. (2024) [16] for a similar structure but much lower (factor 2) than some of the test results of Whitehouse (2004) [11] and Tavouktsoglu (2017) [15]. Obviously, the maximum scour depth along a large-scale caisson structure is strongly dependent on the precise geometry and dimensions of the structure and the prevailing flow and sediment conditions. At the present stage of research, scour predictions for a circular gravity-based structure (GBS) should always be based on the results of physical scale model tests in a laboratory basin in combination with numerical modelling.

Various empirical scour models (relationships) are available for scour predictions around monopiles and jacket structures. However, many of these models/relationships are based on laboratory scour data only, resulting in unreliable time-scale predictions. The semi-empirical SEDSCOUR model proposed in this paper is based on well-known sediment transport predictors for bed load and suspended load transport in laboratory and field conditions, resulting in a reliable time-scale prediction, as shown by the successful scour predictions for various laboratory and field cases with monopiles and jacket structures. It has been shown that the SEDSCOUR model can be used for the reliable prediction of free scour and global scour near monopiles and jacket structures in a sandy bed (even with some mud) but not for large scale caisson-type foundation structures.

The prediction of scour along the flank of a caisson structure requires the use of a more sophisticated morpho-dynamic model, preferably a 3D model operated on a very fine grid. At the present stage of computer power, these models cannot be used for realistic long-term predictions. Therefore, herein, another approach using a detailed 2DV

model with a fine grid along a stream tube following the contour of the caisson was explored. The dimensions of the stream tube can be derived from a 3D-flow model or from laboratory measurements. The SUSTIM2DV model [27,28] simulates the sediment transport in 50 to 100 points over the depth along the stream tube and can be run at a time scale of 1 to 5 years. An application for a caisson with a base diameter of 40 m shows a realistic maximum scour depth of about 5 m on a time scale of a few months. Model runs for monopile structures with storm waves included show that the scour depth is slightly reduced due to sediment deposition in the scour pit during storms, which has also been observed in field conditions (Luchterduinen wind park, The Netherlands).

Author Contributions: Conceptualization and methodology, L.C.v.R. and L.P.; Software and validation, L.C.v.R. and N.G.; Laboratory measurements, D.S.; Resources, L.P.; Data curation, D.S.; Writing—original draft preparation, L.C.v.R.; Writing—review and editing, L.C.v.R.; Supervision, L.P. and L.C.v.R.; Project administration, L.P. All authors have read and agreed to the published version of the manuscript..

Funding: This research received no external funding

Data Availability Statement: All experimental data are available on request.

Conflicts of Interest: The authors declare no conflicts of interest. (no funding involved).

References

1. Breusers, H.N.C.; Nicollet, G.; Shen, H.W. Local scour around cylindrical piers. *J. Hydr. Res.* **1977**, *15*, 211–252.
2. Melville, B.W. *Scour at Bridge Sites*; Civil Engineering Practice, 2; Technomic Publishing Company: Lancaster, PA, USA, 1988; pp. 327–362.
3. Melville, B.W.; Sutherland, A.J. Design method for local scour at bridge piers. *J. Hydraul. Eng. ASCE* **1988**, *114*, 1210–1226.
4. Kothyari, U.C.; Ranga Raju, K.G.; Garde, R.J. Live-bed scour around cylindrical bridge piers. *J. Hydr. Res. IAHR* **1992**, *30*, 701–715.
5. Melville, B.W. Pier and abutment scour: Integrated approach. *J. Hydraul. Eng.* **1997**, *123*, 125–136.
6. Lim, S.Y. Equilibrium clear-water scour around an abutment. *J. Hydraul. Eng.* **1997**, *123*, 237–243.
7. Melville, B.W.; Coleman, S.E. *Bridge Scour*; Water Resources Publications: Littleton, CO, USA, 2000.
8. Rees, J.; Larcombe, P.; Vivian, C.; Judd, A. *Scroby Sands Offshore Wind Farm—Coastal Processes Monitoring*; Cefas Lowestoft Laboratory, Lowestoft, UK, 2006.
9. Rudolph, D.; Raaijmakers, T.; Stam, C.J. Time-dependent scour development under combined current and wave conditions; hindcast of field measurements. In Proceedings of the 4th International Conference on scour and erosion, Tokyo, Japan, 5–7 November 2008.
10. Raaijmakers, T.C.; Van Velzen, G.; Riezebos, H.J. Dynamic scour prediction for offshore monopiles. In Proceedings of 7th International Conference Scour and Erosion, Perth, Australia, 2–4 December 2014.
11. Whitehouse, R.S.J. Marine scour at large foundations. In Proceedings of the 2nd International Conference on Scour and Erosion, Singapore, 14–17 November 2004.
12. Whitehouse, R.; Harris, J.; Sutherland, J.; Rees, J. An assessment of field data for scour at offshore wind turbine foundations. In Proceedings of the Fourth International Conference on scour and erosion, Tokyo, Japan, 5–7 November 2008.
13. Whitehouse, R.; Harris, J.; Sutherland, J. Evaluating scour at marine gravity structures. HR Wallingford. *ICE-Marit. Eng.* **2012**, *164*, 143–157.
14. Simons, R.R.; Weller, J.; Whitehouse, R.J.S. Scour development around truncated cylindrical structures. In *Coastal Structures 2007, Proceedings of the 5th Coastal Structures International Conference, CSt07, Venice, Italy, 2–4 July 2007*; Franco, L.; Tomasicchio, G.R.; Lamberti, A. Eds.; World Scientific: Singapore, 2007; pp. 1881–1891.
15. Tavouktsoglu, N.S.. Scour and Scour Protection Around Offshore Gravity-Based Foundations. Ph.D. Thesis, University College, London, UK, 2017.
16. Sarmiento, J.; Guanche, R.; Losada, I.J.; Serna, J. Experimental analysis of scour around an offshore wind gravity base foundation. *Ocean. Eng.* **2024**, *308*, 118330. https://doi.org/10.1016/j.oceaneng.2024.118330.

17. Rudolph, R.; Bos, K.J.; Luijendijk, A.P.; Rietema, K.; Out, J.M.M. *Scour Around Offshore Structures; Analysis of Field Measurements*; Deltares: Delft, The Netherlands, 2004.
18. Bolle, A.; de Winter, J.; Goossens, W.; Haerens, P.; Dewaele, G. Scour monitoring around offshore jackets and gravity based foundations. In Proceedings of the Sixth International Conference on Scour and Erosion, ICSE 6, Paris, France, 27–31 August 2012.
19. Baelus, L.; Bolle, A.; Szengel, V. Long term scour monitoring around offshore jacket foundations on a sandy seabed. In Proceedings of the Ninth International Conference on Scour and Erosion, ICSE 9, Taipei, Taiwan, 5–8 November 2018.
20. Welzel, M.; Schendel, A.; Schlurmann, T.; Hildebrandt, A. Volume-based assessment of erosion patterns around a hydrodynamic transparent offshore structure. *Energies* **2019**, *12*, 3089. https://doi.org/10.3390/en12163089.
21. Welzel, M.; Schendel, A.; Hildebrandt, A.; Schlurmann, T. Scour development around a jacket structure in combined waves and current conditions compared to monopile foundations. *Coast Eng.* **2019**, *152*, 103515 https://doi.org/10.1016/j.coastaleng.2019.103515.
22. Welzel, M.; Schendel, A.; Goseberg, N.; Hildebrandt, A.; Schlurmann, T. Influence of structural elements on the spatial sediment displacement around a jacket-type offshore foundation. *Water* **2020**, *12*, 1651. https://doi.org/10.3390/w12061651.
23. Welzel, M.; Schlendel, A.; Satari, R.; Neuweiler, I.; Schlurmann, T. Spatio-temporal analysis of scour around complex offshore foundations under clear water and live bed conditions. *Ocean. Eng.* **2024**, *298*, 117042. https://doi.org//10.1016/j.oceaneng.2024.117042.
24. Zhang, J.; Zhang, P.; Guo, Y.; Ji, Y.; Fu, R. Large eddy simulation of the flow field characteristics around a jacket foundation under unidirectional flow actions. *Ocenan Eng.* **2025**, *137*, 120057. https://doi.org/10.1016/j.oceaneng.2024.120057.
25. Chambel, J.; Fazeres-Ferradosa, T.; Miranda, F.; Bento, A.M.; Taveiro-Pinto, F.; Lomonaco, P. A Comprehensive Review on Scour and Scour Protections for Complex Bottom-Fixed Offshore and Marine Renewable Energy Foundations. *Ocean. Eng.* **2024**, *304*, 117829. https://doi.org/10.1016/j.oceaneng.2024.117829.
26. Miles, J.; Martin, T.; Goddard, L. Current and wave effects around windfarm monopile foundations. *Coast. Eng.* **2017**, *121*, 167–178.
27. Van Rijn, L.C.; Meijer, K.; Dumont, K.; Fordeyn, J. Practical 2DV modelling of deposition and erosion of sand and mud in dredged channels due to currents and waves. *J. Waterw. Port Coast. Ocean. Eng*. **2024**, *150*, 04024002. https://doi.org/10.1061/JWPED5.wweng-2065.
28. Van Rijn, L.C.; Meijer, K.; Dumont, K.; Fordeyn, J. Simulation of sand and mud transport processes in currents and waves by time-dependent 2DV model. *Int. J. Sediment Res.* **2024**, *40*, 1–14. https://doi.org/10.1016/j.ijsrc.2024.10.009.
29. Van Rijn, L.C. *Principles of Sediment Transport in Rivers, Estuaries and Coastal Seas*; Aqua Publications: Amsterdam, The Netherlands, 1993
30. Van Rijn, L.C. Unified view of sediment transport by currents and waves, I: Initiation of motion, bed roughness, and bed-load transport. *J. Hydraul. Eng.* 2007, 133,649-667.
31. Van Rijn, L.C.. Unified view of sediment transport by currents and waves, II: Suspended transport. *J. Hydraul. Eng.* **2007**, *133*, 668–389.
32. Sheppard, D.M.; Miller, W. Live-Bed local pier scour experiments. *J. Hydraul. Eng. ASCE* **2006**, *132*, 635–642.
33. Sheppard, D.M. *Large Scale and Live Bed Local Pier Scour Experiments (Phase 1)*; Final Report; Florida Department of Transportation FDOT: Tallahassee, FL, USA, 2003.
34. Deltares. *Scour and Scour Mitigation*; Hollandse Kust Zuid Wind Farm Zone: Delft, The Netherlands, 2017.